



HAL
open science

Imprint of seasonality changes on fluvio-glacial dynamics across Heinrich Stadial 1 (NE Atlantic Ocean)

Wiem Fersi, Aurélie Penaud, Mélanie Wary, Samuel Toucanne, Claire
Waelbroeck, Linda Rossignol, Frédérique Eynaud

► To cite this version:

Wiem Fersi, Aurélie Penaud, Mélanie Wary, Samuel Toucanne, Claire Waelbroeck, et al.. Imprint of seasonality changes on fluvio-glacial dynamics across Heinrich Stadial 1 (NE Atlantic Ocean). *Global and Planetary Change*, 2021, 204, pp.103552. 10.1016/j.gloplacha.2021.103552 . hal-03455758v2

HAL Id: hal-03455758

<https://hal.science/hal-03455758v2>

Submitted on 15 Dec 2021

HAL is a multi-disciplinary open access archive for the deposit and dissemination of scientific research documents, whether they are published or not. The documents may come from teaching and research institutions in France or abroad, or from public or private research centers.

L'archive ouverte pluridisciplinaire **HAL**, est destinée au dépôt et à la diffusion de documents scientifiques de niveau recherche, publiés ou non, émanant des établissements d'enseignement et de recherche français ou étrangers, des laboratoires publics ou privés.

1 **Imprint of seasonality changes on fluvio-glacial dynamics across**
2 **Heinrich Stadial 1 (NE Atlantic Ocean)**

3
4 **Wiem Fersi ^{(a)*}, Aurélie Penaud ^(a), Mélanie Wary ^(b), Samuel Toucanne ^(c), Claire**
5 **Waelbroeck ^(d), Linda Rossignol ^(e), Frédérique Eynaud ^(e)**

6
7 *(a) Univ Brest (UBO), CNRS, UMR 6538 Laboratoire Géosciences Océan (LGO), F-*
8 *29280 Plouzané, France*

9 *(b) Institut de Ciència i Tecnologia Ambientals (ICTA-UAB), Universitat Autònoma de*
10 *Barcelona, Bellaterra, Catalonia, Spain*

11 *(c) Ifremer, Laboratoire Géophysique et environnements Sédimentaires. F-29280*
12 *Plouzané, France*

13 *(d) LOCEAN/IPSL, Sorbonne Université-CNRS-IRD-MNHN, UMR7159, Paris, France*

14 *(e) Univ Bordeaux, CNRS, UMR 5805 Environnements et Paléoenvironnements*
15 *Océaniques et Continentaux (EPOC), F-33405 Talence, France*

16
17 *Corresponding author. Tel.: +33-298-498-741; fax: +33-298-498-760.

18 *E-mail addresses: [wiam.feresi@univ-brest.fr](mailto:wiem.feresi@univ-brest.fr), aurelie.penaud@univ-brest.fr*

19

20

21 **Abstract**

22 The northern Bay of Biscay has previously proven its great potential for recording the *'Fleuve*
23 *Manche'* paleoriver (i.e., the largest Pleistocene river in Europe) fluvio-glacial activity. In this
24 study, new dinoflagellate cyst (dinocyst) analyses have been carried out at sub-centennial
25 resolution in core MD13-3438 to reconstruct the deglacial history of the *'Fleuve Manche'*
26 paleoriver runoff coupled with European Ice Sheets (EIS) fluctuations across Heinrich Stadial
27 1 (HS1: 18.2–14.6 ka BP), a key extreme climatic event of the last glacial period. Prior to
28 Heinrich Event (HE) 1 (16.7–14.6 ka BP), the onset of HS1 (18.2–16.7 ka BP) appears here
29 marked by enhanced *'Fleuve Manche'* paleoriver runoff, materialized by laminated deposits.
30 Our work suggests a novel sub-centennial scale subdivision of the early HS1 (laminated)
31 interval into 5 sub-phases when episodes of substantial fluvio-glacial delivery concomitant
32 with warm summers alternate with episodes of moderate runoff associated with extended cold
33 winters. We argue that multidecadal seasonal changes played a key role in the hydrological
34 regime of western Europe during this HS1 interval, with the retreat of the southern limb of the
35 EIS, and associated influx of meltwater and fluvio-glacial delivery, which were strongly
36 influenced by those multidecadal changes in seasonality. Interestingly, our paleoclimatic
37 record not only evidences the crucial role of seasonality in controlling climate and
38 hydrological variations during HS1 but also shows a remarkable echo with reconstructions
39 from the western Mediterranean Basin, highlighting common climate forcings at regional
40 scale during the last deglaciation.

41 *Keywords: Heinrich Stadial 1; Dinoflagellate cysts; northern Bay of Biscay; 'Fleuve*
42 *Manche' paleoriver; European Ice Sheets*

43

44 **1. Introduction**

45 The last glacial period was accompanied by millennial-scale abrupt climate shifts, portrayed
46 in Greenland ice-cores as rapid transitions from cold atmospheric phases termed Greenland
47 Stadials (GS) to warm atmospheric phases referred to as Greenland Interstadials (GI; e.g.,
48 Dansgaard et al., 1993; Rasmussen et al., 2014). Despite their original designation, these
49 climate excursions had an impact across the globe (e.g., Voelker, 2002). In the North Atlantic
50 Ocean, some GS were associated with massive iceberg surges mainly from the Laurentide Ice
51 Sheet (LIS) *via* the Hudson Strait Ice Stream (e.g., Bond et al., 1992, 1993; Broecker et al.,
52 1992, 1994; Hemming, 2004), identified in marine sediments as Ice Rafted Debris (IRD)-
53 enriched layers (e.g., Bond et al., 1993; Broecker, 1994; Heinrich, 1988). These massive
54 iceberg(and thus freshwater) surge events are known as Heinrich Events (HEs including
55 HE1), with their corresponding stadial phases called Heinrich Stadials (HSs including HS1;
56 Barker et al., 2009; Sanchez Goñi and Harrison, 2010). The associated huge freshwater
57 releases resulted in large reductions of the Atlantic Meridional Overturning Circulation
58 (AMOC; e.g., McManus et al., 2004; Stanford et al., 2006, 2011; Ng et al., 2018; Toucanne et
59 al., 2021). Numerous studies demonstrated that Greenland Iceland and European Ice Sheets
60 were also major contributors to the oceanic disturbances in the North Atlantic Ocean,
61 especially when considering the surge sequencing along time (e.g., Bond et al., 1997, 1999;
62 Grousset et al., 2000, 2001; Hemming et al., 2000, 2004; Knutz et al., 2001, 2007; Hall et al.,
63 2006; Peck et al., 2006; Nygård et al., 2007; Toucanne et al., 2008, 2010, 2015).

64 HS1, including the HE1 layer, occurred at the onset of the last deglaciation (~19-11 ka BP;
65 Clark et al., 2012a), just before the abrupt Bølling-Allerød (B/A) warming event starting at ca.
66 14.7 ka BP (Rasmussen et al., 2014) and after the Last Glacial Maximum (LGM; Mix et al.,
67 2001). Over the LGM, which was characterized by a large European Ice Sheet (EIS) including
68 the British-Irish (BIIS) and Scandinavian (SIS) Ice Sheets, the '*Fleuve Manche*' paleoriver
69 (Channel River) was one of the largest river systems that drained western Europe (e.g.,
70 Gibbard, 1988; Toucanne et al., 2009, 2010, 2015). This huge fluvial system included the
71 French, Belgian and British rivers, and the merged German, Polish and Dutch rivers, on the
72 exposed English Channel and North Sea Basin, respectively. Multiproxy studies conducted
73 along the northwestern European margin and especially from the northern Bay of Biscay (e.g.,
74 Zaragosi et al., 2001; Auffret et al., 2002; Mojtahid et al., 2005, 2017; Eynaud et al., 2007,
75 2012; Penaud et al., 2009; Toucanne et al., 2009, 2010), identified recurrent phases of
76 meltwater inputs at the onset of HS1 (between 18.3 and 17 ka BP). Materialized in sediments

77 as millimeter- to centimeter-scale laminations, they were attributed to the seasonal melting of
78 the EIS and seasonal subsequent freshwater discharge from the '*Fleuve Manche*' paleoriver.
79 Further works provided new evidence of a differential contribution from ice sheets to the
80 laminated deposit, with a particularly large SIS/Baltic sourced part during the last
81 deglaciation and the HS1 interval (Toucanne et al., 2015). Until now, palynological
82 investigation of this laminated facies (Eynaud, 1999, 2007, 2012; Auffret et al., 2000;
83 Zaragosi et al., 2001; Penaud et al., 2009) was performed at resolution varying between 70
84 and 250 years only, due to the strong dilution of palynomorphs in sediments. Such laminated
85 facies, corresponding to exceptionally high sedimentation rates, appear as ideal candidates to
86 increase the temporal resolution of marine records and thus improve our understanding of
87 short-lived fluctuations in the regime of the '*Fleuve Manche*' paleoriver and associated EIS
88 dynamics.

89 Our study thus constitutes the first detailed dinocyst study encompassing the HS1 interval in
90 the Bay of Biscay with a special focus on the laminated facies deposited at the onset of HS1.
91 Our main objective was to decipher the set and sequence of events that occurred during this
92 period over the northern Bay of Biscay. Our high-resolution palynological study was
93 conducted on core MD13-3438 and combined with micropaleontological, geochemical and
94 sedimentological analyses available for the twin reference core MD95-2002. Our multiproxy
95 approach led to:

96 (1) the reconstruction of the coupled EIS and '*Fleuve Manche*' paleoriver dynamics across
97 HS1;

98 (2) the study of high frequency seasonal variability within the laminated deposit, providing
99 the first reconstruction of the sub-centennial climate variability across HS1 in the NE
100 Atlantic;

101 (3) and the characterization of sea surface conditions over the northern Bay of Biscay using
102 dinocyst quantifications (keeping in mind their potentialities and limits in the study area).

103 **2. Environmental context**

104 **2.1. Location of the studied core**

105 The Calypso long piston core MD13-3438 (47°27' N; 8°27' W; 2180 m water depth; 36 m
106 long) and twin core MD95-2002 (47°27' N; 8°32' W; 2174 m water depth) were respectively
107 collected during the VT 133 / MERIADZEK (Woerther, 2013) and MD101-IMAGES
108 (Bassinot and Labeyrie, 1996) oceanographic cruises on board the R/V Marion Dufresne
109 (Table 1).

110 These marine sedimentary archives were retrieved from the Meriadzek Terrace, northern Bay
111 of Biscay, directly off the mouth of the '*Fleuve Manche*' paleoriver (Fig. 1a). Their recovery,
112 on a structure lying 600 m above the abyssal plain, guarantees few disturbances from gravity
113 processes despite the proximity of deep-sea turbidite systems (Auffret et al., 2000; Zaragosi et
114 al., 2000, 2001). The late Quaternary sedimentation of this area was imprinted by supplies
115 from the northwestern European drainage catchments *via* the '*Fleuve Manche*' paleoriver
116 during glacial lowstands (Auffret et al., 2000; Bourillet et al., 2003; Mojtahid et al., 2005;
117 Zaragosi et al., 2006; Eynaud et al., 2007; Toucanne et al., 2008, 2009).

118 At present, the water column is structured by the deep Labrador Sea Water (~1500-2000 m
119 depth) characterized by salinity ranging from 35 to 35.5 psu (Cossa et al., 2004) and the
120 intermediate warm and salty (35.7 psu) Mediterranean Outflow Water (800-1500 m depth).
121 Down to 800 m depth, the modern European Slope Current carries warm and salty waters to
122 the Nordic Seas (Berx et al., 2013). Surface waters over the study area correspond to the
123 southward recirculation of the North Atlantic Current (NAC; Fig. 1a), i.e., the south-eastern
124 branch of the subpolar North Atlantic gyre (e.g., Sutton and Allen, 1997; Daniault et al.,
125 2016). At the study site, modern (i.e., pre-21st century) mean Sea Surface Temperature (SST)
126 and Salinity (SSS) are 11.7±0.6 °C and 35.54±0.05 psu in winter, and 17.5±1.0 °C and
127 35.58±0.10 psu in summer (World Ocean Atlas, 2001; Conkright et al., 2002).

128

129 **2.2. Climatic changes in the northern Bay of Biscay during the last** 130 **40 kyr with focus on HS1**

131 A large number of studies have shown that core MD95-2002 (Fig. 1a) has archived the history
132 of deglacial pulses and meltwater discharge from the EIS (Zaragosi et al., 2001; Ménot et al.,
133 2006; Eynaud et al., 2007, 2012; Penaud et al., 2009; Toucanne et al., 2009, 2015; Fig. 1b).

134 Data acquired on MD95-2002 (Fig. 1b) indeed provided nearshore marine to terrestrial
135 information (Table 1 for related references).

136 In the North Atlantic Ocean, HS can be recognized on the basis of *Neogloboquadrina*
137 *pachyderma* abundances close to 100% (e.g., Broecker et al., 1992; Eynaud et al., 2009). At
138 site MD95-2002, HS1 (blue band on Fig. 1b) is thus identified as the interval between 18.2–
139 14.6 ka BP (Fig. 1b). Early HS1 is evidenced by repeated alternation of millimeter- to
140 centimeter-scale deposits (i.e., laminae) of mud and Coarse Lithic Grains (CLG) (Zaragosi et
141 al., 2001). This facies results from an intense activity of the ‘*Fleuve Manche*’ paleoriver in
142 response to the substantial EIS retreat (e.g., Mojtahid et al., 2005; Zaragosi et al., 2006;
143 Eynaud et al., 2007; Toucanne et al., 2008). This laminated interval is associated with high
144 concentrations of the freshwater micro-algae *Pediastrum* (Penaud et al., 2009), high values of
145 the Ti/Ca-XRF ratio (i.e., detrital *versus* biogenic proxy for enhanced terrigenous supply;
146 Toucanne et al., 2009, 2012, 2015) and of the Branched and Isoprenoid Tetraether (BIT)
147 index (i.e., a proxy for the relative fluvial input of terrestrial organic matter in the marine
148 environment; Ménot et al., 2006). All those tracers highlight strong fluvial inputs and
149 terrestrial-sourced organic sediment advections over the northern Bay of Biscay. This period
150 is concomitant with major EIS melting events, especially from the Baltic Ice Stream of the
151 SIS, accompanied by seasonal spring-summer meltwater discharge into the Bay of Biscay
152 (Zaragosi et al., 2001; Mojtahid et al., 2005; Ménot et al., 2006; Eynaud et al., 2007, 2012;
153 Penaud et al., 2009; Toucanne et al., 2008, 2009, 2015). Within the laminated interval, the
154 concentrations of CLG (Fig.1b) include both, Laurentide and European-sourced IRDs and
155 also fluvial lithic grains transported *via* the ‘*Fleuve Manche*’ paleoriver. Increased CLG
156 concentrations then recorded between 16.7 and 15 ka BP (Fig.1b; Zaragosi et al., 2001)
157 characterize the HE1 phase. This interval contains the ‘conventional’ HE1 layer marked by
158 notable peaks of magnetic susceptibility and carbonates (low Ti/Ca values) at ~16 ka BP
159 characterizing the typical LIS surge (Grousset et al., 2000; Toucanne et al., 2015; Fig.1b).

160

161 **3. Material and methods**

162 **3.1. Stratigraphy of core MD13-3438**

163 The age model of core MD13-3438 is wedged on the last updated chronostratigraphy of core
164 MD95-2002 (Toucanne et al., 2015). This latter was built with the Clam software (Blaauw,
165 2010) by integrating 22 AMS-¹⁴C dates over the last 40 kyr with additional tie-points: (i) 4
166 AMS-¹⁴C dates tied from the neighbouring cores MD03-2690 and MD03-2692, and (ii) *N.*
167 *pachyderma* abundances correlated with the NGRIP $\delta^{18}\text{O}$ signal. Modern reservoir age
168 correction is estimated to about 352 ± 92 years. Prior to HS1 and during the Holocene, the
169 reservoir age constantly averaged around 400 ± 200 ¹⁴C years. During HS1, the B/A and the
170 Younger Dryas, average reservoir ages were respectively estimated to about 970, 680 and 875
171 years with uncertainties of 200 years (1s) (Toucanne et al., 2015).

172 The age model of core MD13-3438 was established by the correlation of its Ti/Ca-XRF signal
173 with that of its twin core MD95-2002 (Fig. 1b). The XRF analysis of core MD13-3438 was
174 performed at Ifremer (Plouzané) using an Avaatech X-Ray Fluorescence core scanner at 1
175 cm-resolution. Tie points used to synchronize both Ti/Ca-XRF signals can be found in Table
176 2. The correlation is supported by planktonic foraminiferal data (counts of the total
177 assemblage performed on the >150 μm sediment fraction and on >300 individuals for each
178 sample at EPOC laboratory), especially the high *N. pachyderma* relative abundances
179 delimiting the HS1 interval (Fig. 1b). Our 5 cm-sampling frequency for dinocyst analyses
180 enables us to achieve a temporal resolution of about 18 to 186 years, with a mean resolution
181 of 58 years in all the studied sections, and of about 29 years in the laminated sequence,
182 characterized by sedimentation rate values around 185 cm/kyr (Fig. 1b). This resolution thus
183 provides valuable new details on the deglacial climatic history of the northern European
184 margin across the HS1 interval.

185 It is worth noting that recent studies showed that the rapid cooling marking the onset of HS1
186 in the North Atlantic took place at $17.48 \text{ ka} \pm 0.21 \text{ ka}$ (1σ) (Missiaen et al., 2019; Waelbroeck
187 et al., 2019) while maximal *N. pachyderma* abundances (i.e., allowing identifying HS 1) in
188 core MD95-2002 between 880-390 cm, and between 575-245 cm in core MD13-3438, start at
189 around 18.2 ka BP (Fig. 1b). Our chronologies are likely too old by about 700 years at the
190 onset of HS1 as a result of underestimated reservoir ages over the last deglaciation.

191

192

193 **3.2. Dinocyst analyses**

194 a. Laboratory procedure, dinoflagellate cyst identification and diversity indices

195 A total of 76 samples were analysed from the 18.4-14 ka BP interval encompassing HS1.
196 Palynological treatments were performed at EPOC laboratory (University of Bordeaux,
197 France) following a standard protocol described by de Vernal et al. (1999). Calibrated tablets
198 of known concentrations of *Lycopodium clavatum* spores were added to each sample before
199 chemical treatments in order to estimate palynomorph concentrations. Chemical treatments
200 include cold HCl (10 %), cold HF (40 and 70%) and sieving through single-use 10 µm nylon
201 mesh screens. For each sample, an average of about 400 specimens (minimal counts of 175
202 cysts) was achieved using a Leica DM 2500 microscope at ×630 magnification except for the
203 laminated sequence between 575 and 330 cm for which an average of 120 specimens
204 (minimal counts of 100 cysts) was obtained due to strong dilution.

205 Dinocyst ecology has been thoroughly described through the progressive development and
206 compilation of atlases of modern cyst distribution (Matthiessen, 1995; Rochon et al., 1999;
207 Marret and Zonneveld, 2003; Zonneveld et al., 2013; van Nieuwenhove et al., 2020; Marret et
208 al., 2020). For this study, taxonomic attribution and the grouping of some species were done
209 in accordance with those atlases. *Brigantedinium* spp. taxa include all spherical brown cysts
210 excluding *Dubridinium* spp. Other peridinioid cysts were grouped (i.e., *Quinquecuspis* spp.,
211 *Lejeunecysta* spp., *Dubridinium* spp. and *Votadinium* spp.) as miscellaneous peridinioid cysts
212 (MPCs). Dinocyst assemblages were described with the relative abundances of each taxon
213 calculated on the basis of the total sum of specimens counted including unidentified taxa and
214 excluding pre-Quaternary cysts. Finally, the species richness and Margalef index (Harper,
215 1999), calculated using PAST v.1.75b (Hammer et al., 2001), have been used to estimate the
216 dinocyst assemblage diversity as an additional ecological indicator. The species richness
217 represents the number of different taxa identified within each studied sample. The Margalef
218 diversity index (Margalef, 1958) is defined by: Margalef's Index = $(S - 1) / \ln(N)$, where S
219 and N correspond to the total number of species (S) and of individuals (N) in the sample.

220

221 b. Dinoflagellate cyst ratios and fluvial-derived palynological tracers

222 A “Warm/Cold” (W/C) ratio (Table 3) was used to qualitatively address SST variations
223 (Turon and Londeix, 1988; Versteegh, 1994; Combourieu- Nebout et al., 1999; Eynaud et al.,
224 2016; Penaud et al., 2016). Also, the “Heterotrophic/Autotrophic” (H/A) ratio (Table 3) was

225 calculated. This ratio is often used to discuss changes in primary productivity (PP) since
226 heterotrophic dinoflagellates have a strict heterotrophic strategy of nutrition, being indirectly
227 related to food resources, especially diatoms (Wall et al., 1977; Lewis et al., 1990; Marret,
228 1994; Zonneveld et al., 1997, 2001, 2013). It is worth noting that a large part of
229 gonyaulacoids cysts (phototrophic cyst producing taxa) may survive thousands of years in
230 well oxygenated sediments but heterotrophic peridinioids are extremely sensitive and
231 vulnerable to early diagenesis. Since availability of oxygen in the sediments is the most
232 important diagenetic variable, it has been suggested that the amount of species-selective
233 degradation (i.e., here calculated as the H/A ratio for instance) may also be related to bottom
234 water oxygen concentration, itself related to the rate of deep-ocean ventilation (Zonneveld et
235 al., 2008). Both PP and/or taphonomic issues have to be taken into account to fully understand
236 the H/A ratio.

237 The “*Lingulodinium machaerophorum* / *Operculodinium centrocarpum*” (Lmac/Ocen) ratio
238 was used to discuss continental *versus* oceanic influences at the core location (e.g., Penaud et
239 al., 2020), *L. machaerophorum* being a taxon dominating (nearly monospecifically) in
240 estuarine environments of the French Atlantic coast (Wall et al., 1977; Morzadec-Kerfourn,
241 1977; Ganne et al., 2016; Lambert et al., 2017). Finally, a new ratio “*L. machaerophorum* /
242 *Islandinium minutum*” (Lmac/Imin) has been used in this study as a proxy for summer *versus*
243 winter prevailing seasonality modes. *I. minutum* is abundant in polar regions where surface
244 waters do not exceed 0 °C in winter (Zonneveld et al., 2013).

245 In addition, pre-Quaternary dinocysts and Non Pollen Palynomorphs (NPP) including
246 freshwater micro-algae *Pediastrum* spp. coenobia, *Botryococcus* spp. and *Concentricystes*
247 spp.) were counted on the same palynological slides and expressed in absolute concentrations
248 (palynomorphs/cm³). It has been demonstrated that *Pediastrum* spp. freshwater micro-algae
249 are related to strong river discharge in marine environments (Zaragosi et al., 2001; Lézine et
250 al., 2005; Eynaud et al., 2007; Penaud et al., 2009). Also, the biostratigraphical study of
251 Kaiser (2001, unpublished data), based on the identification of reworked dinocysts in core
252 MD95-2002 revealed that they were derived from the second half of the Mesozoic (Late
253 Jurassic) to the Early Tertiary (Miocene), then characterizing the *Manche*, Parisian Basin and
254 South England geological formations. Therefore, concentrations of *Pediastrum* spp. micro-
255 algae and pre-Quaternary dinocysts, together with the ratio of “Reworked” (Rd, pre-
256 Quaternary) *versus* “Modern” (Md) dinocysts (i.e., Rd/Md ratio), constitute robust proxies to
257 discuss ‘*Fleuve Manche*’ paleoriver discharge in the Bay of Biscay (e.g., Zaragosi et al.,
258 2001; Kaiser, 2001; Eynaud et al., 2007; Penaud et al., 2009). The Rd/Md ratio, reworked cyst

259 and *Pediastrum* spp. concentrations, together with *L. machaerophorum* occurrences and the
260 Lmac/Ocen ratio will be referred to as Fluvial-derived Palynological Tracers (FPT) allowing
261 discussing fluvio-glacial delivery to the NW European margin.

262

263 c. Dinocyst-based quantitative reconstructions of sea-surface parameters

264 The Modern Analogue Techniques (MAT), run on the “R version 2.7.0” software (R
265 Development Core Team, 2008; <http://www.r-project.org/>), was applied on dinocyst
266 assemblages to estimate past quantitative sea-surface environmental parameters. The MAT
267 consists in the comparison of fossil records with modern dinocyst assemblages from the most
268 recent update of the standardized Northern Hemisphere “modern” dinocyst database, which
269 includes the abundance of 71 different taxa and 1968 sites in relation to 17 modern
270 environmental parameters (de Vernal et al., 2020). This method relies on the assumption that
271 modern relationships between hydrographical parameters and dinocyst assemblages were still
272 valid in the past (e.g., Guiot and de Vernal, 2007). Sources of uncertainties, quantified with
273 the Root Mean Square Errors (RMSE), could derive from the lack of modern analogues
274 corresponding to fossil assemblages (Guiot and de Vernal, 2007; de Vernal et al., 2020).

275 The quantification of hydrological parameters is based on a weighted average of the values
276 obtained for the five best modern analogues, with the maximum weight being given to the
277 statistically closest analogue. Regarding the threshold distance ($d_T=1.2$), analogues are i) good
278 when the distance $d < d_T/2$, ii) acceptable when $d_T/2 < d < d_T$, and iii) poor when $d > d_T$ (de
279 Vernal et al., 2005). The n=1968 database and its related environmental database, allows the
280 reconstruction of summer and winter SST and SSS, mean annual Primary Productivity (PP),
281 and Sea Ice Cover Duration (SIC_D), with RMSE of ± 1.8 °C for SST_{summer}, ± 1.2 °C for
282 SST_{winter}, ± 2.1 psu for SSS_{summer}, ± 1.1 psu for SSS_{winter}, ± 138 gC m⁻² for PP_{annual}, ± 1.5
283 months year⁻¹ for SIC_D.

284

285 **4. Palynological results**

286 Based on a cluster analysis run on dinocyst taxa percentages with the Psimpoll program, 9
287 palynozones were identified in core MD13-3438. We labelled them according to the
288 stratigraphic interval they match: LGM (595-578 cm), HS1-a as the onset of HS1 prior to
289 HE1 – HS1-a being subdivided into 5 sub-palynozones termed HS1-a1 to HS1-a5 (578-330
290 cm), and HS1-b (330-270 cm) and HS1-c (270-240 cm) as the first and second phase of HE1,
291 respectively. Palynological data are presented and discussed according to these palynozones.
292 They are plotted *versus* depth (cm) in result figures (Figs. 2 to 4), to exhibit the regularly
293 sampled data without considering the strong impact of sedimentation rates, and then *versus*
294 age (Cal ka BP) in the discussion figures (Figs. 5 to 7).

295

296 **4.1. Quaternary dinocyst and other palynomorph abundances and** 297 **derived indices**

298 a. General observations on MD13-3438 results

299 A total of 31 different Quaternary dinocyst taxa (autotrophic or heterotrophic) have been
300 identified (Table 3) with a species richness of about 15 different taxa per slide varying
301 between 7 taxa at 580 cm and 25 taxa at 240 cm (Fig. 2). The Margalef index strongly
302 matches the species richness with a general increasing trend from the bottom to the top of the
303 studied section (Fig. 2), diversity being the lowest during the end of the LGM. Quaternary
304 dinocyst concentrations vary from about 1200 to 47600 cysts/cm³, with average values of
305 5200 cysts/cm³ (Fig. 3). Overall, dinocyst assemblages are dominated by heterotrophic taxa
306 (mean value of 57%) including especially *Brigantedinium* spp. (30%) and miscellaneous
307 peridinioid cysts (MPCs) (21%), as well as *Islandinium minutum* (3%), cysts of
308 *Protoperidinium nudum* grouped with *Selenopemphix quanta* (1%) as well as *Echinidinium*
309 spp. (2%; Fig. 3). The H/A ratio trend (Fig. 2) seems to be mainly explained by fluctuations in
310 *Brigantedinium* spp. (Fig. 2). The lowest values of this ratio are observed across the LGM,
311 followed by high to moderate values across HS1-a and by a decreasing trend from the start of
312 HS1-b to the onset of the B/A. Autotrophic taxa (mean value of 43%) are dominated by the
313 following species: *Operculodinium centrocarpum* (16%), *Bitectatodinium tepikiense* (9%),
314 *Lingulodinium machaerophorum* (4%), cysts of *Pentapharsodinium dalei* (3%),
315 *Nematosphaeropsis labyrinthus* (3 %), *Spiniferites lazus* (2%), *Spiniferites ramosus* (2%)
316 *Spiniferites belerius* (2%) and *Spiniferites septentrionalis* (2%) (Fig. 3).

317

318 b. Detailed observations according to the 9 palynozones

319 Each of the 9 palynozones can be described in terms of Quaternary dinocyst percentages,
320 which they were statistically established from, but also in terms of other micropaleontological
321 indicators. They are labelled from LGM to B/A (Fig. 2, Fig. 3):

322 • **LGM**: This lowermost zone exhibits the highest dinocyst concentrations (10000 to 47000
323 cysts/cm³) explained by maximal values of *O. centrocarpum* occurrences (higher than 85%).
324 *N. pachyderma* percentages show relatively low values (lower than 22%).

325 • **HS1-a**: The transition between LGM and HS1-a is marked by an abrupt decrease of *O.*
326 *centrocarpum* percentages and the increase of heterotrophic taxa (*Brigantedinium* spp. and
327 MPCs) representing more than 60% of the total cyst assemblages until 330 cm. Also, this
328 interval is characterized by increasing *N. pachyderma* percentages. Five sub-zones have been
329 distinguished: Sub-zone **HS1-a1** corresponds to the first evidence of increasing FPT values
330 and shows higher percentages of *B. tepikiense*, *Brigantedinium* spp. as well as MPCs. In sub-
331 zone **HS1-a2**, *B. tepikiense* percentages decrease while a diversification of the assemblage is
332 observed, with especially higher relative abundances of *Spiniferites* spp., *L. machaerophorum*
333 and cysts of *P. dalei*, while Quaternary dinocyst concentrations are the highest of the whole
334 HS1-a interval. Importantly, concentrations of reworked cysts and of total freshwater micro-
335 algae show maximal values during this HS1-a2 sub-zone (Fig. 2). Dinocyst concentrations
336 reach minimal values (2500 cyst/cm³) within HS1-a3, HS1-a4 and HS1-a5, when important
337 increases of MPCs are also recorded. While **HS1-a3** is characterized by the dominance of
338 *Brigantedinium* spp., HS1-a4 and HS1-a5 are marked by maximal values of *L.*
339 *machaerophorum* (16%) and the highest Lmac/Ocen values. A second peak of freshwater
340 micro-algae concentrations associated with maximal values of Rd/Md ratio additionally
341 characterises HS1-a4 (Fig. 2). *I. minutum* abundances increase from the beginning of HS1-a5
342 at 360 cm concomitantly with decreasing FPT values (Fig. 2, Fig. 3).

343 • **HS1-b**: This interval is generally characterized by a strong drop of MPCs with low to near-
344 zero values persisting all the way up to the top of the studied interval, and the gradual decline
345 of *L. machaerophorum* percentages. Maximal values of *I. minutum* (maximum about 20%)
346 and *S. septentrionalis* (maximum about 6%) occur in this zone.

347 • **HS1-c**: This interval is characterized by higher percentages of *O. centrocarpum* (20%), *B.*
348 *tepikiense* (18%), and *Echinidinium* spp. (10%), while *I. minutum* and *L. machaerophorum*
349 strongly decrease and are nearly absent until the end of the studied sequence.

350 • **B/A:** This interval is marked by the significant drop of *N. pachyderma* percentages from
351 ~95% to ~35%. Dinocyst assemblages are characterized by the quasi-total disappearance of
352 MPCs as well as significant percentages of *N. labyrinthus* (~15%). The first part of the B/A
353 interval is characterized by increasing percentages of *Brigantedinium* spp. and occurrences of
354 *Impagidinium* spp., while the second part of B/A (lowest *N. pachyderma* abundances) is
355 characterized by increasing *B. tepikiense* and cysts of *P. dalei* percentages.

356

357 **4.2. Dinocyst-based sea-surface quantifications**

358 a. General observations on MD13-3438 results

359 Our MAT-based reconstructions rely on one to five modern analogues (Fig. 4a). Overall (76
360 samples in total), 5 samples are scored as “good” (especially within the basal LGM interval
361 and at the top of the B/A interval) and 45 samples are scored as “acceptable” and range
362 between the threshold distance ($d_T=1.2$) and $d_T/2$ (Fig. 4a). Samples scoring as “poor” are
363 more particularly found within HS1-b and HS1-c, intervals also characterized by fewer
364 analogues. Fig. 4a shows that the d_T pattern is very close to that of the H/A ratio.
365 Consequently, uncertainties in dinocyst quantifications are likely related with heterotrophic
366 taxa occurrences and especially with the high abundances of the *Brigantedinium* spp. cysts.

367 From the $n=1968$ modern dinocyst database (de Vernal et al., 2020), 30 modern analogues are
368 selected as the best analogues during the MAT calculations. They are mainly distributed along
369 the eastern and western northern coasts of Canada, eastern coasts of USA, along the eastern
370 and western coasts of Greenland and in the northern Atlantic Ocean, as well as in the
371 Norwegian and Arctic Seas (Fig. 4b). Boxes have been delimited in Fig. 4b to show the main
372 locations of those best analogues across each time interval in Fig. 4a (color code at the right
373 of the figure). Within the end of the LGM, best analogues are located in the western coasts of
374 Canada and in the Norwegian Sea. Most of the modern analogues selected within HS1-a are
375 located in the eastern coasts of USA and Canada. For HS1-b, analogues are located in the
376 eastern and western coasts of Greenland and Svalbard. Analogues found within HS1-c are
377 more diversified and located in the eastern coasts of USA, Canada and Greenland and in the
378 North Sea, this latter representing the principal source of modern analogues for the upper B/A
379 interval (Figs. 4a and b).

380

381 b. Dinocyst-based sea surface parameters estimates

382 Dinocyst-derived mean summer SSTs (Fig. 4a) vary between -0.9 and 29.6 °C (average of
383 17.3 °C) and mean winter SSTs (Fig. 4a) range between -1.8 and 18.5 °C (average of 7.3 °C).
384 SST_{summer} and SST_{winter} values show similar trends, with their highest values recorded within
385 HS1-a (SST_{summer} of 20 °C and SST_{winter} of 9 °C). These atypically elevated values, especially
386 for SST_{summer}, exceed modern mean SSTs for the northern Bay of Biscay (modern average
387 SST_{summer} of 17.5 and SST_{winter} of 11.7°C). This zone is characterized by strong occurrences
388 of heterotrophic taxa (*Brigantedinium* spp. and MPCs), as also highlighted by the high H/A
389 ratio (Fig. 2), and modern analogues have been found along the eastern coasts of USA in
390 subtropical areas also characterized by highly productive (strong fluvial discharge) conditions
391 (modern analogue value of PP_{annual} around 1800 gC m⁻²).

392 Dinocyst-derived SSS_{summer} and SSS_{winter} (Fig. 4a) show low salinities along the studied
393 section ranging between 25 and 34 psu (average of 30 psu), below mean average modern
394 values of about 35.6 psu over the northern Bay of Biscay. The lowest salinities are recorded
395 during the laminated interval HS1-a with SSS_{summer} values of 29 psu, consistent with strong
396 fluvial discharge such as observed today on the eastern coasts of USA where analogues were
397 selected (Figs. 4a, b). The highest SSS values (around 34 psu) are recorded in the B/A
398 interval.

399 Although quantifications are especially critical within HS1-b because of the lack of modern
400 analogues across this interval (i.e., only 3 over 11 levels provided parameter estimates based
401 on MAT), this latter appears characterized by maximal Sea Ice Cover duration (“SIC_D” of ca.
402 10 months per year; Fig. 4a) and the lowest SST_{summer} and SST_{winter} (ca. 5 °C and -2 °C,
403 respectively; Fig. 4a). Finally, reconstructed PP_{annual} appears the highest within HS1-a (950
404 gC m⁻²; Fig. 4a).

405 **5. The Last Deglaciation on the northern Bay of Biscay**

406 Our compilation of MD13-3438 multiproxy signals indicative of fluvial discharge, allows us
407 to describe for the first time the consequence of those hydrographic events at sub-centennial
408 scale over the period covering the LGM to the B/A in the northern Bay of Biscay. We
409 superimpose to our new and high-resolution results some of those previously published and
410 established at lower temporal resolution (but longer time-scale) from twin core MD95-2002,
411 (Fig. 5; Fig. 6; Zaragosi et al., 2001), and highlight the additional information provided by our
412 new palynological study.

413

414 **5.1. The warm climatic conditions bracketing HS1**

415 Although the LGM and B/A are not the main targeted periods of our study, with consequently
416 few samples documenting those intervals in core MD13-3438, it is important to describe the
417 climatic context bracketing the main period of focus HS1. We thus, in the following, have
418 synthesized information consistent with earlier works (especially including those relying on
419 longer time-scale and multiproxy MD95-2002 records) and their derived climatic
420 interpretations.

421 a. The end of the LGM

422 This interval is characterized by extremely low abundances of *N. pachyderma* (Figs. 5 and 6)
423 and the highest percentages of *O. centrocarpum* (Fig. 6), considered to be a tracer of the NAC
424 (Turon, 1984; Eynaud et al., 2004, 2012; Penaud et al., 2008, 2009). It is also associated with
425 relatively high SST_{winter} (~9°C; Fig. 6) and high SSS (~34 psu; Fig. 6; see also Eynaud et al.,
426 2012, focused on LGM salinities derived from multiproxy records). Those relatively warm
427 conditions were suggested to be induced by a significant penetration of the warm and salty
428 NAC in the Bay of Biscay (Eynaud, 1999; Zaragosi et al., 2001; Eynaud et al., 2007, 2012;
429 Penaud et al., 2009) and more generally a more vigorous NAC in the NE Atlantic Ocean
430 (Weinelt et al., 1996; Rosell-Melé and Comes, 1999; Kucera et al., 2005; de Vernal et al.,
431 2000, 2002, 2005, 2006; Caille et al., 2013; Wary et al., 2015).

432 In parallel, a slight increase of the ‘*Fleuve Manche*’ paleoriver activity is recorded (through
433 higher concentrations of reworked palynomorphs – Zaragosi et al., 2001 – and slight increase
434 of the BIT-index and C/N ratio – Ménot et al., 2006; Fig. 5), synchronously with the 19-ka
435 meltwater pulse identified in Europe by significant melting of the BIIS in Ireland (K-MWP:

436 Kilkeel event; Clark et al., 2004; Fig. 7) and of the southern SIS (i.e., R4 event; Toucanne et
437 al., 2015; Fig. 7), while summer insolation at 65°N increases (Berger and Loutre, 1991; Fig.
438 7). In core MD13-3438, the end of the LGM displays small amounts of terrestrial organic
439 matter exported to the northern Bay of Biscay and moderate marine productivity as suggested
440 by low to moderate values of inferred PP, moderate MPCs (Fig. 5) and the lowest values of
441 *Brigantedinium* spp. cyst percentages (Fig. 3).

442

443 b. The onset of the B/A

444 The onset of this relatively warm interval is characterized by a remarkable decrease in polar
445 foraminiferal *N. pachyderma* percentages (Figs. 5 and 6) accompanied by a significant
446 increase of *N. labyrinthus* percentages (Fig. 6) and a brief incursion of *Impagidinium* spp.
447 (Fig. 3). Also, increases of dinocyst concentrations are coeval with a moderate TOC/N ratio in
448 core MD95-2002 (Ménot et al., 2006; Fig. 5) suggesting a moderate PP increase. Since 14.6
449 ka BP, warmer sea-surface conditions (high SST_{winter} close to modern ones and high W/C
450 ratio; Fig. 6) are associated with a rapid SSS increase (about 34 psu; Fig. 6) highlighting a
451 vigorous NAC with warm and salty Atlantic surface waters carried to the study area,
452 consistent with a concomitant strong AMOC as depicted in various records from the whole
453 North Atlantic Ocean (e.g. McManus et al., 2004; Ng et al., 2018; Fig. 7). Data acquired in
454 the northern North Atlantic (Caulle et al., 2013; Wary et al., 2015), the western Iberian
455 margin (Bard et al., 2000; Martrat et al., 2007; Eynaud et al., 2009; Hodell et al., 2013;
456 Salgueiro et al., 2014; Naughton et al., 2016) and the Alboran Sea (Cacho et al., 1999; Martrat
457 et al., 2014; Català et al., 2019) support this observation of warmer conditions at a regional
458 scale. It appears accompanied by rapid forest development as documented in the western
459 Mediterranean borderlands and NW Iberia at the onset of the B/A (Naughton et al., 2007,
460 2016; Fletcher and Sanchez-Goñi, 2008; Combourieu-Nebout et al., 2009; Camuera et al.,
461 2019, 2021; Fig. 7) concomitant with increasing humidity, as also identified in speleothem
462 records from southwestern Europe (Genty et al., 2006; Moreno et al., 2010; Jalut et al., 2010).
463 An increase in seaward transfer of fluvially-derived sediments is reported directly north of the
464 Meriadzek Terrace ca. 16-14 ka, indicating possible influence of the retreating Irish Ice Sheet
465 (which is not connected to the 'Fleuve Manche' paleoriver) at that time (Toucanne et al.,
466 2008). However, our data show no such evidence of deglacial meltwater fluxes at site MD13-
467 3438, neither with FPT values (only a slight increase of *Pediastrum* spp. concentrations; Fig.
468 5) nor with the BIT-index (Ménot et al., 2006; Fig. 5). This lack of deglacial evidence on the
469 Meriadzek Terrace may be explained by the major episode of sea-level rise referred to as

470 “Meltwater Pulse 1A” (MWP-1A, Fig. 7) which occurred at around ~14.6-14.3 ka BP. This
471 led to a ~20 m sea-level rise in less than 500 years (Weaver et al., 2003; Deschamps et al.,
472 2012; Lambeck et al., 2014; Fig. 7) probably responsible for the displacement of the ‘*Fleuve*
473 *Manche*’ mouth about 300 km eastward (Toucanne et al., 2012, 2010), thus rapidly halting
474 any ‘*Fleuve Manche*’ imprint on the sedimentary record of our study site.

475

476 **5.2. A sub-centennial subdivision of HS1 in the northern Bay of** 477 **Biscay**

478 a. Early-HS1, laminated interval (HS1-a): 18.2-16.7 ka BP

479 **General observations**

480 Overall, the HS1-a interval is characterized by a huge increase in terrigenous sediment
481 supplies in the study area, evidenced through higher values of the Ti/Ca-XRF ratio (Fig. 5)
482 and higher sedimentation rates (mean values of about 200 cm/kyr at the study site) at site
483 MD13-348, as well as through maximal values of the BIT-index (core MD95-2002; Ménot et
484 al., 2006; Fig. 5) and low CLG concentrations mainly due to dilution by terrigenous sediment
485 at site MD95-2002. This interval is also marked by a reduction of *O. centrocarpum*
486 percentages from about 90% to 10 % and increasing percentages of *Spiniferites* spp. (i.e., *S.*
487 *bentorii* and *S. lazus*), which point to a transition from a full-oceanic (end of the LGM) to a
488 neritic to coastal influence (cf. Penaud et al., 2020 for modern ecological requirements of
489 dinocyst taxa in the study area) with enhanced PP (Fig. 5). This is also confirmed by high
490 values of the Lmac/Ocen ratio (Fig. 7) and, in general, by the substantial rise of FPT values.
491 These indications support the progradation of a large outer-shelf delta on the margin at that
492 time and huge delivery of the ‘*Fleuve Manche*’ sediment load close to the Meriadzek Terrace
493 (Toucanne et al., 2012). Geochemical investigations suggested that the meltwater release
494 pattern is mainly related to the Baltic Ice Stream of the SIS (R5 event; Toucanne et al., 2015;
495 Fig. 7).

496 Enhanced proximal fluvio-glacial delivery from the ‘*Fleuve Manche*’ paleoriver was
497 suggested to result from the seasonal influx of meltwater from the retreating EIS and
498 responsible for the formation of the laminated facies (Zaragosi et al., 2001, 2006; Mojtahid et
499 al., 2005; Ménot et al., 2006; Eynaud et al., 2007, 2012; Toucanne et al., 2008, 2009; Penaud
500 et al., 2009; Fig. 7). Here, dinocyst-derived quantitative reconstructions further show a
501 significant drop of SSS, especially of SSS_{summer} (mean values about 29 psu; Fig. 6), with a
502 large seasonal SSS amplitude (>2 psu; Fig. 6), suggesting that the EIS melting occurred

503 mainly during the spring-summer season (Mojtahid et al., 2005; Toucanne et al., 2009, 2015;
504 Eynaud et al., 2012; see Fig. 8 for a conceptual scheme of past hydrographic changes in the
505 study area).

506 The HS1-a interval is characterized by a sustainable increase in the H/A ratio (fig. 7).
507 Interestingly, this pattern matches the AMOC trend (cf. $^{231}\text{Pa}/^{230}\text{Th}$ values; McManus et al.,
508 2004; Ng et al., 2018; Fig.7) with high values of heterotrophic cysts during the AMOC
509 slowdown in the North Atlantic Ocean and conversely. This observation highlights the
510 probable taphonomic issue linked to varying bottom water ventilation (Zonneveld et al.,
511 2008). In our study, heterotrophics (Fig. 5) may be related to either increasing PP and/or
512 better preservation of peridinioid cysts under low bottom-water oxygenation. Remarkably,
513 benthic foraminiferal taxa, from the northern Bay of Biscay, indicated both a general
514 eutrophication and a severe bottom water dysoxia in the sea floor (Mojtahid et al., 2017).
515 Overall cold and dry conditions are observed in the southern and western Iberian Peninsula,
516 with a strong reduction of the Mediterranean and temperate forests (Fletcher and Sanchez
517 Goñi, 2008; Naughton et al., 2016; Camuera et al., 2021; Fig.7) and a notable increase of
518 xerophytic taxa (i.e., steppic taxa) (Camuera et al., 2021; Fig.7).

519

520 ***Sub-centennial variability of fluvio-glacial discharge on northern Bay of Biscay***

521 Our unprecedented high-resolution multiproxy study of the laminated facies shows a new sub-
522 centennial-scale structure, following a multi-step scenario encompassing 5 intervals (Figs. 5
523 to 7; cf. subsection 4.1). Enhanced fluvial inputs were recorded within HS1-a2 corresponding
524 to maximal terrestrial advection and HS1-a4 consisting to the strongest stratification level of
525 the surface water column and the strongest westward shift of the freshwater front toward the
526 ocean (Fig. 5). Interestingly, these intervals are characterized by lower and fluctuating *N.*
527 *pachyderma* percentages and increased values of SST and seasonality reconstructed from
528 dinocysts at site MD13-3438, testifying warm sea-surface conditions (Fig. 6). Decreased
529 fluvial discharge marked the HS1-a1, HS1-a3 and HS1-a5 intervals, this latter appears
530 characterized by the establishment of cold sea surface conditions in the northern Bay of
531 Biscay within the latter.

532 The oscillating pattern of 'Fleuve Manche' paleoriver runoff illustrated here by the different
533 phases identified in HS1-a finds a striking echo in the environmental fluctuations from arid to
534 more humid conditions in the Iberian Peninsula between 18.4 and 16.4 ka BP (Camuera et al.,
535 2021: Fig. 7), with phases of higher runoff matching those of increased humidity in southern

536 Europe. Furthermore, these observations are regionally supported by SST records from the
537 Alboran Sea (Cacho et al., 1999, 2006; Martrat et al., 2014; Fig.7).

538

539 ***The role of multidecadal changes in seasonality on fluvio-glacial fluxes to the northern***
540 ***Bay of Biscay***

541 The first conceptual model proposed by Mojtahid et al. (2005) suggested: (i) enhanced
542 melting of EIS and surrounding glaciers, responsible for enhanced clay and CLG fluxes to the
543 Bay of Biscay *via* the '*Fleuve Manche*' paleoriver during spring and especially summer
544 seasons, and (ii) freezing SST and sea-ice cover establishment inhibiting EIS melting during
545 winter seasons. While first studies attributed CLG-rich units to the seasonal calving of EIS
546 icebergs onto the northern Bay of Biscay (Mojtahid et al., 2005; Zaragosi et al., 2006; Eynaud
547 et al., 2007), Toucanne et al (2009) later proposed that the episodic rainout of these particular
548 CLG originates instead from the '*Fleuve Manche*' paleoriver discharge of anchor-ice (i.e., ice
549 attached to the riverbed) and of sediment-rich frazil-ice (Reimnitz and Kempama, 1987;
550 Kempama et al., 2001).

551 Echoing the seasonal dynamic of the '*Fleuve Manche*' paleoriver, our data interestingly
552 suggest warmer sea-surface conditions within HS1-a (mean SST values about $\sim 9^{\circ}\text{C}$ and high
553 values of the W/C ratio; Figs. 6) associated with a significant temperature seasonality increase
554 ($> 12^{\circ}\text{C}$; Fig. 6), especially within periods of maximal fluvial discharge, namely HS1-a2 and
555 HS1-a4. To further investigate this, we specifically created a 'summer *versus* winter index' as
556 the ratio between two major dinocyst taxa occurring regionally and illustrating two opposite
557 environmental dynamics: the estuarine taxon *L. machaerophorum* and the polar taxon *I.*
558 *minutum* (Lmac/Imin ratio; Fig.7). We consider *L. machaerophorum*, whose highest
559 abundances at present are encountered in areas under strong fluvial influence, as
560 characteristics of the '*Fleuve Manche*' paleoriver discharge induced by European ice sheet
561 retreat and melting during the deglaciation, i.e., which occurred preferentially during summer
562 seasons according to earlier sedimentological studies cited above. In contrast, occurrences of
563 the polar species *I. minutum* are associated with cold sea-surface conditions and expansion of
564 temporary sea-ice cover (1-3 months/year, Fig. 6) over the studied interval in the northern
565 Bay of Biscay (as it is at present at high latitudes), then mostly expressing a winter signal
566 (Fig. 8).

567 The Lmac/Imin ratio (Fig. 7) matches the seasonality signal (Fig. 6). It shows high values
568 within most of the HS1-a interval and particularly during maximal runoff periods HS1-a2 and
569 HS1-a4. On the contrary, intervals characterized by lower fluvio-glacial inputs (HS1-a1, HS1-

570 a3 and HS1-a5) depict low L_{mac}/I_{min} values, highlighting the limited influence of summer
571 seasons and the prevalence of cold winters (Fig. 8). We thus argue that multidecadal changes
572 of the seasonality pattern played a substantial role on the EIS and ‘*Fleuve Manche*’ paleoriver
573 sub-centennial dynamics during the last deglaciation, with release of river ice and meltwater
574 via the ‘*Fleuve Manche*’ paleoriver favoured during episodes with prevailing summer mode,
575 and reversely formation of anchor- and frazil-ice in the ‘*Fleuve Manche*’ paleoriver favoured
576 during episodes of winter prevailing mode (see Fig. 8 for a conceptual scheme of past
577 hydrographic changes in the study area).

578 Such an enhanced warm summer-prevailing mechanism could then explain the EIS melting,
579 as far as in the northern European lowlands, in an ‘apparent’ long cold climate stadial (Fig. 8).
580 HS1 is generally seen as a very cold and dry interval in the North Atlantic Ocean and across
581 Europe (Bard et al., 2000), marked by overall light NGRIP $\delta^{18}O$ values, especially during
582 HE1 (Fig. 7). The strong changes in SST seasonality observed in the northeastern Atlantic
583 Ocean, and weakly expressed in high latitudes, may then support the hypothesis that
584 Greenland temperatures mainly represent winter temperatures (Denton et al., 2005, 2010;
585 Buizert et al., 2014, 2018). However, it is worth noting the occurrence of a plateau of slightly
586 lighter NGRIP $\delta^{18}O$ values over the HS1-a interval (Fig. 7) arguing for slightly warmer
587 atmospheric conditions.

588

589 b. Late-HS1, namely HE1 layer (HS1-b and HS1-c): 16.7–14.6 ka BP

590 In our study, at 16.7 ka BP, the onset of HE1 phase is characterized by the disappearance of
591 laminae deposits as well as a drastic drop of sedimentation rates (from 156 to 41 cm/kyr; Fig.
592 5) and in the BIT-index (Ménot et al., 2006; Fig. 5). Those changes are associated with a
593 substantial decline of FPT values including the L_{mac}/O_{cen} ratio. All these observations point
594 to a considerable decrease of the ‘*Fleuve Manche*’ paleoriver runoff. Also, high values of
595 $C_{37:4}$ alkenones (i.e., a biomarker derived from haptophyte algae, and used as a proxy for low
596 salinity water associated with icebergs; Ménot et al., 2006) are synchronous with high CLG
597 concentrations (Fig. 6). The local hydrology is thus strongly impacted by both Laurentide-
598 and European-derived icebergs at that time (Grousset et al., 2000). Increasing percentages of
599 the polar species *I. minutum* (Fig. 6), recognized as a good tracer of cold surface waters
600 seasonally to quasi-permanently covered with sea-ice (Zonneveld et al., 2013; Radi et al.,
601 2013), are synchronous with low reconstructed SST_{winter} (Fig. 6) indicating cold sea-surface
602 conditions (Fig. 6).

603 Dinocyst assemblages enabled us to determine two sub-zones, HS1-b and HS1-c, with a 120
604 years study resolution on the entire HE1 interval:

605 **HS1-b (16.7–15.6 ka BP; 85 years study resolution)** is characterized by the drastic decrease
606 of fluvial inputs (low FPT values, Fig. 5; decreasing L_{mac}/O_{cen} ratio, Fig. 7). Maximal *I.*
607 *minutum* (Fig. 6) and *S. septentrionalis* (Fig. 3) occurrences are recorded at 16.4 ka BP,
608 depicting the coldest conditions (Figs. 6 and 7). Low *O. centrocarpum* percentages
609 additionally suggest a still weakened NAC, consistently with $^{231}Pa/^{230}Th$ record which
610 suggests that a weakened AMOC state persisted for over a millennium (~16.5–15 ka BP) in
611 the North Atlantic Ocean (Ng et al., 2018; Fig. 7). These cold surface conditions recorded on
612 the northern Bay of Biscay may have been responsible for a weaker EIS melting and are
613 consistent with records from the IRD belt indicating a widespread cooling associated with a
614 major calving episode of the LIS (Stanford et al., 2011; Hodell et al., 2017). This interval is
615 indeed marked by a notable peak of magnetic susceptibility (Figs. 5 and 6) and significant
616 CLG concentrations (core MD95-2002; Figs. 5 and 6) accompanied by minimal values of the
617 Ti/Ca-XRF ratio at 16 ka BP (Fig. 5) indicative of carbonate-rich CLG (Auffret et al., 1996;
618 Toucanne, 2009;). This may correspond to the ‘cemented marls’ of Hemming (2004)
619 interpreted as the LIS (i.e., Hudson Strait) iceberg delivery to the North Atlantic Ocean
620 (Toucanne et al., 2015).

621 Extremely cold conditions at our study site (Figs. 6, 7 and 8) are synchronous with extremely
622 cold boreal temperatures (lightest NGRIP $\delta^{18}O$ values of the entire HE1 phase; Fig. 7) and
623 with the coldest and most arid environments documented in marine palynological sequences
624 from the Alboran Sea (Combourieu-Nebout et al., 2002, Fletcher and Sanchez Goñi, 2008;
625 Fig7) and off the Iberian Peninsula (Turon et al., 2003; Naughton et al., 2007, 2009, 2016).
626 The dryness over the Mediterranean borderlands increased (Morellón et al., 2009; Camuera et
627 al., 2019; Fig. 7) in relation with the southward migration of the polar front (Eynaud et al.,
628 2009).

629 **HS1-c (15.6–14.6 ka BP; 170 years study resolution)** is characterized by higher percentages
630 of *B. tepikiense* and *P. dalei* cysts, currently observed in surface sediments from the subpolar
631 North Atlantic basin (Harland, 1983; de Vernal et al., 1992; Dale, 1996; Rochon et al., 1999),
632 and also clearly accompanied by both decreasing *I. minutum* percentages and CLG
633 concentrations (Figs. 5 and 6) as well as increasing *O. centrocarpum* percentages (Fig. 3).
634 This suggests warm sea-surface conditions (Fig. 6) with increased thermal seasonal
635 amplitudes (Figs. 6, 7 and 8). The retreat of winter sea-ice marks the end of the HS1 interval
636 in the northeastern Atlantic Ocean. Increasingly warm conditions on the northern Bay of

637 Biscay are consistent with an intensified NAC and increasing SSTs as detected at regional
638 scale (e.g., Caille et al., 2013; Wary et al., 2015; Naughton et al., 2016; Hodell et al., 2013;
639 Cacho et al., 1999; Martrat et al., 2014; Català et al., 2019). Also, warmer and more humid
640 conditions are observed in the southern and western Iberian Peninsula (Fletcher and Sanchez
641 Goñi, 2008; Naughton et al., 2009, 2016; Camuera et al., 2021; Fig.7) that may be attributed
642 to the northward displacement of the polar front (Cayre et al., 1999; Naughton et al., 2009,
643 2016).

644 **6. Conclusion**

645 The high-resolution palynological investigation of the last deglaciation in core MD13-3438
646 (northern Bay of Biscay) highlights significant climatic and paleoenvironmental changes
647 related to both the proximal European Ice Sheets (EIS) and the '*Fleuve Manche*' paleoriver
648 dynamics. Dinocyst-based quantitative reconstructions provide an evaluation of past
649 hydrographical changes. Seven short-scale sub-phases within the HS1 interval were identified
650 for the first time on the northern Bay of Biscay:

651 **HS1-a** (i.e., laminated interval; 18.2–16.7 ka BP) is generally characterized by marked
652 multidecadal changes in the seasonality range, i.e., warm summers resulting in enhanced EIS
653 melting and '*Fleuve Manche*' paleoriver runoff, causing the largest drop of SSS and cold
654 winters resulting in freezing conditions and lower '*Fleuve Manche*' paleoriver activity.
655 Fluvial-derived palynological tracers indicate that this interval is subdivided into five sub-
656 phases. Two maximal meltwater episodes (HS1-a2, 17.8–17.6 ka BP and HS1-a4, 17.4–17 ka
657 BP) are detected, with substantial erosional processes in the '*Fleuve Manche*' basin and
658 strong stratification of the water column. Both events correspond to strong seasonality phases
659 dominated by summer-prevailing modes. Fluvio-glacial discharge of the '*Fleuve Manche*'
660 paleoriver, although significant, is comparatively moderate during HS1-a1 (18.2–17.8 ka BP),
661 HS1-a3 (17.6–17.4 ka BP) and HS1-a5 (17–16.7 ka BP), and possibly result from a decrease
662 of the seasonality that could have limited the EIS melting at that time. Indeed, our new data
663 suggest winter-prevailing modes at that time.

664 **HS1-b** (i.e., first phase of HE1; 16.7–15.6 ka BP) includes the Laurentide-sourced IRDs
665 recorded at ~16 ka BP. This interval is characterized by a substantial decrease of proximal
666 fluvial inputs and cold winters. Cooling sea-surface conditions are recorded with seasonal
667 winter sea-ice cover occurrences and the lowest reconstructed SSTs.

668 **HS1-c** (i.e., second phase of HE1; 15.6–14.6 ka BP) is characterized by warmer sea-surface
669 conditions, suggesting the advection of Atlantic surface waters conveyed by the NAC and
670 leading to the transition to the warm B/A.

671 Our reconstructed sub-centennial variability suggests the crucial role of multidecadal seasonal
672 changes, especially within the early HS 1 interval, for fluvio-glacial dynamics and the melting
673 of the EIS. Furthermore, our records are in agreement with marine and terrestrial sequences
674 from the western Mediterranean basin suggesting common regional forcings acting on the
675 multi-scale climate variability across the last deglaciation.

676

677

678 **7. Acknowledgments**

679 This work was supported by the French projects: ANR IDEGLACE, INSU RISCC, INSU
680 ICE-BIO-RAM and by the European Research Council ERC grant ACCLIMATE/n° 339108.
681 This work results from regional, national and international collaborations, between LGO
682 laboratory (Brest University,), Ifremer (GM), EPOC laboratory (Bordeaux University,),
683 LOCEAN and the Universitat Autònoma of Barcelona. We received funding from the CG29
684 (*Conseil Général du Finistère*, 29) and financial support from LGO and EPOC laboratories.
685 This work was also supported by ISblue project, Interdisciplinary graduate school for the blue
686 planet (ANR-17-EURE-0015) and co-funded by a grant from the French government under
687 the program "Investissements d'Avenir". We thank Mikael Rovere and Patrice Woerther for
688 their assistance onboard the R/V Marion Dufresne, Muriel Georget (EPOC) and Pierre-Olivier
689 Coste (LGO) for their help and laboratory assistance. Mélanie Wary's contribution was also
690 supported through funding from the Spanish Ministry of Science, Innovation and Universities,
691 through the "María de Maeztu" program for Units of Excellence (MDM-2015-0552). We
692 gratefully acknowledge reviewers, whose anonymous comments have contributed to increase
693 the quality of this manuscript.

694

695

696 **8. Table caption**

697 **Table 1:** Datasets acquired on both cores MD95-2002 and MD13-3438 with their
698 corresponding references.

699

700 **Table 2:** List of tie points defined by aligning the Ti/Ca-XRF signal of the well-dated core
701 MD95-2002 with that of the studied core MD13-3438.

702

703 **Table 3:** List of identified autotrophic and heterotrophic dinocyst taxa according to their
704 ecological preferences: cold surface-waters (in blue; C) and warm surface-waters (in orange;
705 W). The Warm/Cold qualitative temperature index is based on these W and C species.

706

707

708 **9. Figure captions**

709 **Figure 1:** Paleogeographic reconstruction of western Europe during the LGM (~ 20 ka BP)
710 modified from Toucanne et al. (2015) and records of the past fluvial activity of the '*Fleuve*
711 *Manche*' paleoriver. **a)** The yellow star corresponds to the location of the study core MD13-
712 3438 and of the core MD95-2002. Black lines represent the extension of the Northern
713 Hemisphere ice caps: (1) the European Ice Sheet (EIS) including the Scandinavian (SIS) and
714 British-Irish Ice Sheets (BIIS) (Boulton et al., 2001; Clark et al., 2012b; Ehlers et al., 2011),
715 with their main fluvio-glacial paths (black arrows), as well as the Alpine Ice Sheet; and (2)
716 the Laurentide Ice Sheet (LIS) with main fluvio-glacial path (white arrow). The bold white
717 arrow identifies the drainage of the '*Fleuve Manche*' paleoriver. The North Atlantic surface
718 circulation (red arrows for the warmer North Atlantic Current (NAC) and its branches) is also
719 shown with the return flow pathway of the deep waters (blue arrows). White shading indicates
720 the extent of the EIS and LIS. The trajectory of the icebergs from the LIS are represented
721 with light blue arrows and white arrows indicate the main supply sources of freshwater to the
722 North Atlantic. **b)** Interval from 40 to 5 ka BP: July insolation at 65°N (Berger and Loutre,
723 1991), Greenland $\delta^{18}\text{O}$ record (GICC05; Svensson et al., 2008, in black), Ti/Ca- XRF data
724 and *N. pachyderma* abundances of core MD13-3438 (in blue) compared with the MD95-2002
725 dataset (identified with red dotted lines and full shaded red) including: *N. pachyderma*
726 abundances (Zaragosi et al., 2001), coarse lithic grain concentrations (CLG; 10^3 grains/g dry
727 sed.; Zaragosi et al., 2001), magnetic susceptibility of bulk sediment (U em ; Grousset et al.,
728 2000), fluvial input proxies (number of laminae per cm and concentrations of freshwater
729 micro-algae *Pediastrum* spp. ; Zaragosi et al., 2001) and the branched and isoprenoid
730 tetraether (BIT) index (Ménot et al., 2006). Light grey band represents the LGM (23–19 ka
731 BP) while blue band allows visualizing HS1 in both cores MD95-2002 and MD13-3438
732 (18.4–14 ka BP). Dark grey band represents the conventional HE1 layer occurring at ~16 ka
733 BP.

734
735 **Figure 2:** Palynological data against depth (cm) with taxonomical indices (species richness,
736 black; Margalef index, grey), percentages of the most abundant taxa *Brigantedinium* spp.,
737 ratio between Heterotrophic and Autotrophic (H/A) dinocysts (grey), percentages of *L.*
738 *machaerophorum*, ratio between *L. machaerophorum* and *O. centrocarpum* (grey),
739 concentrations of reworked dinocysts (blue) and of total freshwater microalgae (dark grey
740 line: including *Botryococcus* spp. (purple), *Concentricystes* spp. (pink) and *Pediastrum* spp.

741 (green)). The reworked (pre-Quaternary) vs. modern (in situ) cyst ratio (Rd/Md) is
742 highlighted in grey. Horizontal lines delineate the nine palynozones / climatic subdivisions
743 discussed in the manuscript. LGM: Last Glacial Maximum; HS1-a1 to HS1-a5: Laminated
744 interval; HS1-b and HS1-c: Heinrich Event 1; B/A: Bølling/Allerød.

745

746 **Figure 3:** Diagram of dinocyst assemblages (i.e., major taxa with values higher than 2% at
747 least once in palynological assemblages) *versus* depth (cm) for core MD13-3438, compared
748 with the relative abundances of the planktonic foraminiferal species *N. pachyderma* and with
749 total dinocyst concentrations (black line) including autotrophic (black dotted line) and
750 heterotrophic (grey dotted line) taxa (cysts/cm³). Red and black stars indicate AMS-¹⁴C dates
751 obtained from cores MD95-2002 and MD03-2690 (Eynaud et al., 2012; Mojtahid et al., 2005;
752 Toucanne et al., 2008; 2015; Zaragosi et al., 2006; Zaragosi et al., 2001) respectively, and
753 grey star refers to the NGRIP tie point used for the MD95-2002 age model. These ages are
754 here projected as equivalent depths for core MD13-3438 using the twins Ti/Ca-XRF signals
755 of both MD95-2002 and MD13-3438 cores (Fig. 1b). Palynozones/climatic subdivisions were
756 based on dinocyst clustering established by Psimpoll program. Horizontal lines delineate the
757 nine palynozones discussed in the manuscript (same as in Fig. 2). High percentages of
758 dinocyst taxa are shown by orange vertical arrows for long-lasting periods and by dotted
759 orange vertical arrows for short periods.

760

761 **Figure 4: a)** Dinocyst-based environmental parameters reconstructed for core MD13-3438
762 with the Modern Analog Technique (MAT) using the n=1968 modern dinocyst database (de
763 Vernal et al., 2020) *versus* depth: SST and SSS for the summer (thin red dotted line) and
764 winter (thick blue dotted line), PP_{annual} (black dotted line), and Sea Ice cover Duration
765 (months/year; grey dotted line). Number of analogues found for each assemblage (minimum
766 of 0 and maximum of 5 allowed with the MAT; dark red). Distances between fossil MD13-
767 3438 assemblages and their “closest” modern analogue (i.e., D_{min}). Threshold distance value
768 ($d_T=1.2$; red line) for quantification robustness: good analogues if D_{min} is between 0 (perfect
769 analogue) and $d_T/2$ (orange line); acceptable analogues if D_{min} is between 0.6 and $d_T=1.2$,
770 and poor analogues (i.e. caution with quantifications) if D_{min} > d_T (de Vernal et al., 2005).
771 Horizontal lines delineate the nine palynozones / climatic subdivisions discussed in the
772 manuscript (same as in Fig. 2 and 3). **b)** Map showing the geographical distribution of the
773 closest analogues (i.e., corresponding to D_{min}) selected by the MAT for the studied section of
774 core MD13-3438 (environmental dataset also from de Vernal et al., 2020). Analogues have

775 been grouped according to geographical areas (color code for boxes; also repeated in Fig. 4a
776 for source area of closest analogues in each palynozone).

777

778 **Figure 5:** Deglacial records of the ‘*Fleuve Manche*’ paleoriver activity on the northern Bay of
779 Biscay between 18.4 and 14 ka BP. For core MD13-3438 (in blue): *N. pachyderma*
780 percentages, sedimentation rates (cm/kyr), Ti/Ca-XRF ratio, freshwater microalgae
781 *Pediastrum* spp. concentrations (10^3 algae/cm³), reworked dinocyst concentrations (10^3
782 cysts/cm³), *L. machaerophorum* percentages and concentrations (10^3 cysts/cm³),
783 reconstructed PP_{annual} (10^3 g C m⁻²) and peridinioid cyst concentrations (10^3 cysts/cm³). For
784 core MD95-2002 (identified with red dotted lines and full shaded red): *N. pachyderma*
785 percentages, coarse lithic grain concentrations CLG (10^3 grain/g dry sed.), number of laminae
786 (laminae/cm), Reworked *versus* Modern dinocyst ratio (Rd/Md, shaded red), *L.*
787 *machaerophorum* percentages (shaded red) (Zaragosi et al., 2001), magnetic susceptibility of
788 bulk sediment (U em; Grousset et al., 2000), Ti/Ca-XRF ratio (Toucanne et al., 2015),
789 branched and isoprenoid tetraether (BIT index; Ménot et al., 2006) and Carbon/Nitrogen ratio
790 (C/N; Ménot et al., 2006). Grey bands correspond to the periods of maximal fluvio-glacial
791 discharges within the HS1-a interval. Horizontal lines delineate the palynozones / climatic
792 subdivisions discussed in the manuscript (same as in Fig. 2, 3 and 4).

793

794 **Figure 6:** Reconstructed hydrological parameters derived from dinocyst assemblages of the
795 core MD13-3438 (in blue, this study) compared with data from MD95-2002 (identified with
796 red dotted lines and full shaded red; Zaragosi et al., 2001). *N. pachyderma* percentages, coarse
797 lithic grain concentrations CLG, magnetic susceptibility of bulk sediment (U em ; Grousset et
798 al., 2000), and number of laminae are compiled with relative abundances of the main dinocyst
799 species, percentages of C37:4 among C37 alkenones (red, Ménot et al., 2006), Warm/Cold
800 dinocyst ratio (W/C, This study), dinocyst-derived sea-surface parameters of MD13-3438
801 (Sea Surface Temperatures: SST_{winter} in blue, SST_{summer} in orange; Sea Surface Salinity:
802 SSS_{summer-winter}; Seasonality (SST_{summer}–SST_{winter}). Grey bands correspond to the periods of
803 maximal fluvio-glacial discharges within the HS1-a interval. Horizontal lines delineate the
804 palynozones / climatic subdivisions discussed in the manuscript (same as in Fig. 2, 3, 4 and
805 5).

806

807 **Figure 7:** Synthesis of main information regarding regional paleoclimatic reconstructions for
808 the last deglaciation and our climate subdivisions especially within HS1.

809 Composite Relative Sea Level (RSL) curve (Lambeck et al., 2014) with identified K-MWP at
810 19 ka BP and MWP-1A at ~14.6 ka BP, July Insolation curve at 65°N (Berger and Loutre,
811 1991), $\delta^{18}\text{O}$ NGRIP record (GICCO05; Svensson et al., 2008), $^{231}\text{Pa}/^{230}\text{Th}$ signal (Ng et al.,
812 2018), *N. pachyderma* percentages (blue, this study; red dotted line for the core MD95-2002
813 (Zaragosi et al., 2001)), H/A ratio (blue, this study; and reversed for comparison along the
814 $^{231}\text{Pa}/^{230}\text{Th}$ signal), Runoff events (R) 4 and 5 (core MD95-2002, Toucanne et al., 2015), *L.*
815 *machaerophorum* versus *O. centrocarpum* (Lmac/Ocen ratio, This study), *L.*
816 *machaerophorum* versus *I. minutum* (Lmac/Imin ratio, This study), dinocyst-derived sea-
817 surface seasonality (SSTsummer–SSTwinter) and three-point moving average of Xerophyte
818 and Mediterranean forest percentages from southern Spain (Camuera et al., 2021) as well as
819 temperate forest percentages from the Alboran Sea (Fletcher and Sanchez Goñi, 2008). The
820 proposed comparison respects dating uncertainties and strong reservoir age impacts at that
821 time may be responsible for generating temporal offsets between records.

822 Dashed grey lines correspond to original values, whereas continuous lines correspond to
823 smoothed data. Grey bands correspond to the periods of maximal fluvio-glacial discharges
824 within the HS1-a interval.

825

826 **Figure 8:** Conceptual model illustrating hydrological conditions and processes involved for
827 fluvio-glacial dynamics across the HS1 interval in the northern Bay of Biscay.

828

829

830 **10. Appendix caption**

831 **Appendix:** Exhaustive table of palynological results (percentages, concentrations and
832 reconstructed parameters)

833

834 **11. References**

- 835 Andersen, K. K., Svensson, A., Johnsen, S. J., Rasmussen, S. O., Bigler, M., Röthlisberger,
836 R., et al., 2006. The Greenland ice core chronology 2005, 15-42 kyr. Part 1:
837 constructing the time scale. *Quat. Sci. Rev.* 25, 3246–3257.
- 838 Auffret, G.A., Boelaert, A., Vergnaud-Grazzini, C., Muller, C., Kerbrat, R., 1996.
839 Identification of Heinrich layers in core KS 01 North-Eastern Atlantic (46°N, 17°W),
840 implications for their origin. *Mar. Geol.* 131, 5–20.

841 Auffret, G., Zaragosi, S., Voisset, M., Droz, L., Loubrieu, B., Pelleau, P., Savoye, B.,
842 Bourillet, J.-F., Baltzer, A., Bourquin, S., Dennielou, B., Coutelle, A., Weber, N.,
843 Floch, G., 2000. First observations on the morphology and recent sedimentary
844 processes of the Celtic Deep Sea Fan [Premieres observations sur la morphologie et
845 les processus sedimentaires recents de l'Eventail celtique]. *Oceanologica Acta* 23,
846 109–116.

847 Auffret, G., Zaragosi, S., Dennielou, B., Cortijo, E., Van Rooij, D., Grousset, F., Pujol, C.,
848 Eynaud, F., Siegert, M., 2002. Terrigenous fluxes at the Celtic margin during the last
849 glacial cycle. *Mar. Geol.* 188, 79–108.

850 Bard, E., Rostek, F., Turon, J.L., Gendreau, S., 2000. Hydrological impact of Heinrich events
851 in the subtropical Northeast Atlantic. *Science* 289, 1321–1324.

852 Barker, S., Diz, P., Vautravers, M. J., Pike, J., Knorr, G., Hall, I. R., Broecker, W. S., 2009.
853 Interhemispheric Atlantic seesaw response during the last deglaciation. *Nature* 457,
854 1097–1102.

855 Bassinot, F., Labeyrie, L., 1996. IMAGES I, MD101: A coring cruise of the R/V Marion
856 Dufresne in the North Atlantic Ocean and Norwegian Sea. Les rapports de campagnes
857 à la mer. Institut Paul-Emile Victor (IPEV).

858 Berger, A., Loutre, M.F., 1991. Insolation values for the climate of the last 10 million years.
859 *Quat. Sci. Rev.* 10, 297–317.

860 Berx, B., Hansen, B., Østerhus, S., Larsen, K. M., Sherwin, T., Jochumsen, K., 2013.
861 Combining in-situ measurements and altimetry to estimate volume, heat and salt
862 transport variability through the Faroe Shetland Channel. *Ocean Science Discussions*,
863 10.

864 Blaauw, M., 2010. Methods and code for ‘classical’ age-modelling of radiocarbon sequences.
865 *Quat. Geochronol.* 5, 512–518.

866 Bond, G.W., Heinrich, H., Broecker, W., Labeyrie, L., McManus, J., Andrews, J., Huon, S.,
867 Jantschik, R., Clasen, S., Simet, C., Tedesco, K., Klas, M., Bonani, G., Ivy, S., 1992.
868 Evidence for massive discharges of icebergs into the North Atlantic Ocean during the
869 last glacial period. *Nature* 360, 245–249.

870 Bond, G., Broecker, W., Johnsen, S., McManus, J., Labeyrie, L., Jouzel, J., Bonani, G., 1993.
871 Correlations between climate records from North Atlantic sediments and Greenland
872 ice. *Nature* 365, 143–147.

873 Bond, G., Showers, W., Cheseby, M., Lotti, R., Almasi, P., deMenocal, P., Priore, P., Cullen,
874 H., Hajdas, I., Bonani, G., 1997. A pervasive millennial-scale cycle in North Atlantic
875 Holocene and glacial climates. *Science* 278, 1257–1266.

876 Bond, G., Showers, W., Elliot, M., Evans, M., Lotti, R., Hajdas, I., Bonani, G., Johnson, S.,
877 1999. The north Atlantic's 1-2 kyr climate rhythm: relation to Heinrich events,
878 Dansgaard/Oeschger cycles and the little ice age. In: Clark, P.U., Webb, R.S.,
879 Keigwin, L.D. (Eds.), *Mechanisms of Global Climate Change at Millennial Time*
880 *Scales*. American Geophysical Union, Washington, D.C, 35–58.

881 Boulton, G.S., Dongelmans, P., Punkari, M., Broadgate, M., 2001. Paleoglaciology of an ice
882 sheet through a glacial cycle: the European ice sheet through the Weichselian. *Quat.*
883 *Sci. Rev.* 20, 591–625.

884 Bourillet, J.-F., Reynaud, J.-Y., Baltzer, A., Zaragosi, S., 2003. The 'Fleuve Manche': the
885 submarine sedimentary features from the outer shelf to the deep-sea fans. *J. Quat. Sci.*
886 18, 261–282.

887 Broecker, W., Bond, G., Klas, M., Clark, E., McManus, J., 1992. Origin of the northern
888 Atlantic's Heinrich events. *Clim. Dyn.* 6, 265–273.

889 Broecker, W.S., 1994. Massive iceberg discharges as triggers for global climate change.
890 *Nature* 372, 421–424.

891 Buizert, C., Gkinis, V., Severinghaus, J. P., He, F., Lecavalier, B. S., Kindler, P., et al., 2014.
892 Greenland temperature response to climate forcing during the last deglaciation.
893 *Science* 345, 1177–1180.

894 Buizert, C., Keisling, B. A., Box, J. E., He, F., Carlson, A. E., Sinclair, G., De Conto, R. M.,
895 2018. Greenland-wide seasonal temperatures during the last deglaciation. *Geophys.*
896 *Res. Lett.* 45, 1905–1914.

897 Cacho, I., Grimalt, J. O., Pelejero, C., Canals, M., Sierro, F. J., Flores, J. A., Shackleton, N.,
898 1999. Dansgaard-Oeschger and Heinrich event imprints in Alboran Sea
899 paleotemperatures. *Paleoceanography* 14, 698–705.

900 Cacho, I., Shackleton, N., Elderfield, H., Sierro, F. J., Grimalt, J. O., 2006. Glacial rapid
901 variability in deep-water temperature and $\delta^{18}\text{O}$ from the Western Mediterranean Sea.
902 *Quat. Sci. Rev.* 25, 3294–3311.

903 Camuera, J., Jimenez-Moreno, G., Ramos-Román, M.J., García-Alix, A., Toney, J.L.,
904 Anderson, R.S., Jimenez-Espejo, F., Bright, J., Webster, C., Yanes, Y., 2019.
905 Vegetation and climate changes during the last two glacial-interglacial cycles in the

906 western Mediterranean: a new long pollen record from Padul (southern Iberian
907 Peninsula). *Quat. Sci. Rev.* 205, 86–105.

908 Camuera, J., Jiménez-Moreno, G., Ramos-Román, M. J., García-Alix, A., Jiménez-Espejo, F.
909 J., Toney, J. L., Anderson, R. S., 2021. Chronological control and centennial-scale
910 climatic subdivisions of the Last Glacial Termination in the western Mediterranean
911 region. *Quat. Sci. Rev.* 255, 106814.

912 Català, A., Cacho Lascorz, I., Frigola Ferrer, J. I., Pena, L. D., Lirer, F., 2019. Holocene
913 hydrography evolution in the Alboran Sea: A multi-record and multiproxy
914 comparison. *Clim. Past.* 15, 927–942.

915 Caille, C., Penaud, A., Eynaud, F., Zaragosi, S., Roche, D. M., Michel, E., Boulay, S.,
916 Richter, T., 2013. Sea-surface hydrographical conditions off South Faeroes and within
917 the North-Eastern North Atlantic through MIS 2: The response of dinocysts. *J. Quat.*
918 *Sci.* 28, 217–228.

919 Cayre, O., Lancelot, Y., Vincent, E., 1999. Paleoceanographic reconstructions from
920 planktonic foraminifera off the Iberian Margin: temperature, salinity, and Heinrich
921 events. *Paleoceanography* 14, 384–396.

922 Clark, P.U., McCabe, A.M., Mix, A.C., et al. 2004. Rapid rise of sea level 19,000 years ago
923 and its global implications. *Science* 304, 1141–1144.

924 Clark, P. U., Shakun, J. D., Baker, P. A., et al., 2012a. Global climate evolution during the
925 last deglaciation. *Proc. Natl. Acad. Sci.* 109, 1134–1142.

926 Clark, C.D., Hughes, A.L.C., Greenwood, S.L., Jordan, C., Sejrup, H.S., 2012b. Pattern and
927 timing of retreat of the last British-Irish Ice Sheet. *Quat. Sci. Rev.* 44, 112–146.

928 Combourieu Nebout, N., Londeix, L., Baudin, F., Turon, J. L., Von Grafenstein, R., 1999.
929 Quaternary marine and continental paleoenvironments in the western Mediterranean
930 (Site 976, Alboran Sea): palynological evidence. In *Proceedings of the Ocean Drilling*
931 *Program. Scientific Results* 161, 457–468.

932 Combourieu-Nebout N., Turon, J. L., Zahn, R., Capotondi, L., Londeix, L., Pahnke, K., 2002.
933 Enhanced aridity and atmospheric high-pressure stability over the western
934 Mediterranean during the North Atlantic cold events of the past 50 ky. *Geology* 30,
935 863–866.

936 Combourieu-Nebout, N., Peyron, O., Dormoy, I., Desprat, S., Beaudouin, C., Kotthoff, U.,
937 Marret, F., 2009. Rapid climatic variability in the west Mediterranean during the last
938 25 000 years from high resolution pollen data. *Clim. Past.* 5, 503–521.

939 Conkright, M. E., Locarnini, R. A., Garcia, H. E., O'Brien, T. D., Boyer, T. P., Stephens, C.,
940 Antonov, J. I., 2002. World Ocean Atlas 2001: Objective analyses, data statistics, and
941 figures: CD-ROM documentation.

942 Cossa, D., Cotté-Krief, M. H., Mason, R. P., Bretaudeau-Sanjuan, J. J. M. C., 2004. Total
943 mercury in the water column near the shelf edge of the European continental margin.
944 *Marine Chemistry* 90, 21–29.

945 Danialt, N., Mercier, H., Lherminier, P., Sarafanov, A., Falina, A., Zunino, P., et al., 2016.
946 The northern North Atlantic Ocean mean circulation in the early 21st century.
947 *Progress in Oceanography* 146, 142–158.

948 Dale, B., 1996. Dinoflagellate cyst ecology: modeling and geological applications. In: J.
949 Jansonius and D.C. McGregor (Editors), *Palynology: principles and applications*, Vol.
950 3. AASP Foundation, Salt Lake City, 1249–1275.

951 Dansgaard, W., Johnsen, S. J., Clausen, H. B., Dahl-Jensen, D., Gundestrup, N. S., Hammer,
952 C. U., Hvidberg, C. S., Steffensen, J. P., Sveinbjörnsdottir, A. E., Jouzel, J., Bond, G.,
953 1993. Evidence for general instability of past climate from a 250-kyr ice-core record.
954 *Nature* 364, 218–220.

955 de Vernal, A., Harland, R., 1992. Quaternary organic-walled dinoflagellate cysts of the North
956 Atlantic Ocean and adjacent seas: ecostratigraphy and biostratigraphy. In “Neogene
957 and Quaternary Dinoflagellate Cyst of the North Atlantic Ocean and Adjacent Seas:
958 Ecostratigraphy and Biostratigraphy” (M. J. Head and J. H. Wrenn, Eds.), pp. 289–
959 328. American Association of Stratigraphic Palynologists Foundation, Dallas.

960 de Vernal, A., Henry, M., Bilodeau, G., 1999. Technique de préparation et d’analyse en
961 micropaléontologie. *Les Cahiers du GEOTOP* vol. 3, Université du Québec à
962 Montréal, Montréal, Canada.

963 de Vernal, A., Hillaire-Marcel, C., Turon, J.-L., Matthiessen, J., 2000. Reconstruction of sea-
964 surface temperature, salinity, and sea-ice cover in the northern North Atlantic during
965 the last glacial maximum based on dinocyst assemblages. *Can. J. Earth Sci.* 37, 725–
966 750.

967 de Vernal, A., Hillaire-Marcel, C., Peltier, W.R., Weaver, A.J., 2002. The structure of the
968 upper water column in the northwest North Atlantic: modern vs. Last Glacial
969 Maximum conditions. *Paleoceanography* 17, 1050.

970 de Vernal, A., Eynaud, F., Henry, M., Hillaire-Marcel, C., Londeix, L., Mangin, S.,
971 Matthiessen, J., Marret, F., Radi, T., Rochon, A., Solignac, S., Turon, J.-L., 2005.
972 Reconstruction of sea-surface conditions at middle to high latitudes of the Northern

973 Hemisphere during the Last Glacial Maximum (LGM) based on dinoflagellate cyst
974 assemblages. *Quat. Sci. Rev.* 24, 897–924.

975 de Vernal, A., Rosell-Melé, A., Kucera, M., Hillaire-Marcel, C., Eynaud, F., Weinelt, M.,
976 Dokken, T., Kageyama, M., 2006. Comparing proxies for the reconstruction of LGM
977 sea-surface conditions in the northern North Atlantic. *Quat. Sci. Rev.* 25, 2820–2834.

978 de Vernal, A., Radi, T., Zaragosi, S., Van Nieuwenhove, N., Rochon, A., Allan, E., et al.,
979 2020. Distribution of common modern dinoflagellate cyst taxa in surface sediments of
980 the Northern Hemisphere in relation to environmental parameters: The new n= 1968
981 database. *Mar. Micropaleontol.* 101796.

982 Denton, G.H., Alley, R.B., Comer, G.C., Broecker, W.S., 2005. The role of seasonality in
983 abrupt climate change. *Quat. Sci. Rev.* 24, 1159–1182.

984 Denton, G.H., Anderson, R.F., Toggweiler, J.R., Edwards, R.L., Schaefer, J.M., Putnam,
985 A.E., 2010. The last glacial termination. *Science* 328, 1652–1656.

986 Deschamps, P., Durand, N., Bard, E., Hamelin, B., Camoin, G., Thomas, A. L., et al., 2012.
987 Ice-sheet collapse and sea-level rise at the Bølling warming 14,600 years ago. *Nature*
988 483, 559–564.

989 Ehlers, J., Gibbard, P.L., Hughes, P.D., 2011. *Quaternary Glaciations e Extent and*
990 *Chronology*, vol. 15. Elsevier, Amsterdam, pp. 1126.

991 Eynaud, F., 1999. *Kystes de dinoflagelle's et evolution paléoclimatique et paléohydrologique*
992 *de l'Atlantique Nord au cours du Dernier Cycle Climatique du Quaternaire*, Ph.D.
993 thesis, 291 pp. Univ. of Bordeaux 1, Bordeaux, France.

994 Eynaud, F., Turon, J. L., Duprat, J., 2004. Comparison of the Holocene and Eemian
995 palaeoenvironments in the South Icelandic Basin: dinoflagellate cysts as proxies for
996 the North Atlantic surface circulation. *Rev. Palaeobot. Palynol.* 128, 55–79.

997 Eynaud, F., Zaragosi, S., Scourse, J.D., Mojtahid, M., Bourillet, J.F., Hall, I.R., Penaud, A.,
998 Locascio, M., Reijonen, A., 2007. Deglacial laminated facies on the NW European
999 continental margin: the hydrographic significance of British Ice sheet deglaciation and
1000 Fleuve Manche paleoriver discharges. *Geochem. Geophys. Geosyst.* 8, Q06019.

1001 Eynaud, F., De Abreu, L., Voelker, A., Schönfeld, J., Salgueiro, E., Turon, J. L., et al., 2009.
1002 Position of the Polar Front along the western Iberian margin during key cold episodes
1003 of the last 45 ka. *Geochem. Geophys. Geosyst.* 10, Q07U05.

1004 Eynaud, F., Malaizé, B., Zaragosi, S., de Vernal, A., Scourse, J., Pujol, C., et al., 2012. New
1005 constraints on European glacial freshwater releases to the North Atlantic Ocean.
1006 *Geophys. Res. Lett.* 39.

1007 Eynaud, F., Londeix, L., Penaud, A., Sanchez-Goni, M. F., Oliveira, D., Desprat, S., Turon, J.
1008 L., 2016. Dinoflagellate cyst population evolution throughout past interglacials: Key
1009 features along the Iberian margin and insights from the new IODP Site U1385 (Exp
1010 339). *Glob. Planet. Chang.* 136, 52–64.

1011 Fensome, R. A., Williams, G. L., 2004. The Lentin and Williams index of fossil
1012 dinoflagellates, 2004 edition. In: AASP Foundation Contributions Series 42, pp. 909.

1013 Fletcher, W.J., Sanchez Goñi, M.F., 2008. Orbital- and sub-orbital-scale climate impacts on
1014 vegetation of the western Mediterranean basin over the last 48,000 yr. *Quat. Res.* 70,
1015 451–464.

1016 Ganne A., Leroyer C., Penaud A., Mojtahid M., 2016. Present-day palynomorph deposits in
1017 an estuarine context: the case of the Loire Estuary. *Journal of Sea Research* 118, 35–
1018 51.

1019 Genty, D., Blamart, D., Ghaleb, B., Plagnes, V., Causse, C., Bakalowicz, M., Zouari, K.,
1020 Chkir, N., Hellstrom, J., Wainer, K., Bourges, F., 2006. Timing and dynamics of the
1021 last deglaciation from European and North African $\delta^{13}C$ stalagmite profiles of
1022 comparison with Chinese and South Hemisphere stalagmites. *Quat. Sci. Rev.* 25,
1023 2118–2142.

1024 Gibbard, P. L., 1988. The history of the great northwest European rivers during the past three
1025 million years. *Philosophical Transactions of the Royal Society of London. B,*
1026 *Biological Sciences* 318, 559–602.

1027 Grousset, F.E., Pujol, C., Labeyrie, L., Auffret, G., Boelaert, A., 2000. Were the North
1028 Atlantic Heinrich events triggered by the behaviour of the European ice sheets?
1029 *Geology* 28, 123–126.

1030 Grousset, F.E., Cortijo, E., Herve, L., Richter, T., Burdloff, D., Duprat, J., Weber, O., 2001.
1031 Zooming in on Heinrich layers. *Paleoceanography* 16, 240–259.

1032 Guiot, J., de Vernal, A., 2007. Transfer functions: methods for quantitative paleoceanography
1033 based on microfossils. In: Hillaire-Marcel (Ed.), *Proxies in Late Cenozoic*
1034 *Paleoceanography. Developments in Marine Geology* 1. Elsevier, pp. 523–563.

1035 Hall, I.R., Moran, S.B., Zahn, R., Knutz, P.C., Shen, C.-C., Edwards, R.L., 2006. Accelerated
1036 drawdown of meridional overturning in the late-glacial Atlantic triggered by transient
1037 pre-H event freshwater perturbation. *Geophys. Res. Lett.* 33, L16616.

1038 Hammer, Ø., Harper, D. A., Ryan, P. D., 2001. PAST: Paleontological statistics software
1039 package for education and data analysis. *Palaeontologia electronica* 4, 9.

1040 Harland, R., 1983. Distribution maps of Recent dinoflagellate cysts in bottom sediments from
1041 the North Atlantic Ocean and adjacent seas. *Palaeontology* 26, 321–387.

1042 Harper, D. A., 1999. Numerical palaeobiology: computer-based modelling and analysis of
1043 fossils and their distributions. John Wiley & Sons Inc.

1044 Harrison, S. P., Goñi, M. S., 2010. Global patterns of vegetation response to millennial-scale
1045 variability and rapid climate change during the last glacial period. *Quaternary Science*
1046 *Reviews* 29, 2957–2980.

1047 Heinrich, H., 1988. Origin and consequences of cyclic ice rafting in the Northeast Atlantic
1048 Ocean during the past 130,000 years. *Quat. Res.* 29, 142-152.

1049 Hemming, S.R., Bond, G.C., Broecker, W.S., Sharp, W.D., Klas-Mendelson, M., 2000.
1050 Evidence from $^{40}\text{Ar}/^{39}\text{Ar}$ ages of individual hornblende grains for varying Laurentide
1051 sources of iceberg discharges 22,000 to 10,500 yr B.P. *Quat. Res.* 54, 372–383.

1052 Hemming, S.R., 2004. Heinrich events: massive late Pleistocene detritus layers of the North
1053 Atlantic and their global climate imprint. *Rev. Geophys.* 42, RG1005, 1–43.

1054 Hodell, D., Crowhurst, S., Skinner, L., Tzedakis, P. C., Margari, V., Channell, J. E., et al.,
1055 2013. Response of Iberian Margin sediments to orbital and suborbital forcing over the
1056 past 420 ka. *Paleoceanography* 28, 185–199.

1057 Hodell, D. A., Nicholl, J. A., Bontognali, T. R., Danino, S., Dorador, J., Dowdeswell, J. A., et
1058 al., 2017. Anatomy of Heinrich Layer 1 and its role in the last deglaciation.
1059 *Paleoceanography* 32, 284–303.

1060 Ivanovic, R. F., Gregoire, L. J., Burke, A., Wickert, A. D., Valdes, P. J., Ng, H. C., et al.,
1061 2018. Acceleration of northern ice sheet melt induces AMOC slowdown and northern
1062 cooling in simulations of the early last deglaciation. *Paleoceanography and*
1063 *Paleoclimatology* 33, 807–824.

1064 Jalut, G., Turu i Michels, V., Dedoubat, J.J., Otto, T., Ezquerro, J., Fontugne, M., Belet, J.M.,
1065 Bonnet, L., García de Celis, A., Redondo-Vega, J.M., Vidal-Romaní, J.R., Santos, L.,
1066 2010. Palaeoenvironmental studies in NW Iberia (Cantabrian range): vegetation
1067 history and synthetic approach of the last deglaciation phases in the western
1068 Mediterranean. *Palaeogeogr. Palaeoclimatol. Palaeoecol.* 297, 330–350.

1069 Kaiser, J., 2001. Caractérisation palynologique des flux terrigènes Manche-Golfe de
1070 Gascogne au cours du Dernier Maximum Glaciaire et du réchauffement Holocène.
1071 *Maîtrise des Sciences de l'Environnement*, Univ. Bordeaux 1, Bordeaux, France, 30
1072 pp.

1073 Kempama, E.W., Reimnitz, E., Barnes, P.W., 2001. Anchor-ice formation and ice rafting in
1074 southwestern Lake Michigan, U.S.A. *Journal of Sedimentary Research* 71, 346–354.

1075 Knutz, P.C., Austin, W.E.N., Jones, E.J.W., 2001. Millennial-scale depositional cycles related
1076 to British Ice Sheet variability and North Atlantic paleocirculation since 45 yr B. P.,
1077 Barra Fan, U. K. margin. *Paleoceanography* 16, 53–64.

1078 Knutz, P.C., Zahn, R., Hall, I.R., 2007. Centennial-scale variability of the British Ice Sheet:
1079 implications for climate forcing and Atlantic meridional overturning circulation during
1080 the last deglaciation. *Paleoceanography* 22, PA1207.

1081 Kucera, M., Weinelt, M., Kiefer, T., Pflaumann, U., Hayes, A., Weinelt, M., et al., 2005.
1082 Reconstruction of sea-surface temperatures from assemblages of planktonic
1083 foraminifera: multi-technique approach based on geographically constrained
1084 calibration data sets and its application to glacial Atlantic and Pacific Oceans. *Quat.*
1085 *Sci. Rev.* 24, 951–998.

1086 Lambeck, K., Rouby, H., Purcell, A., Sun, Y., Sambridge, M., 2014. Sea level and global ice
1087 volumes from the Last Glacial Maximum to the Holocene. *Proceedings of the National*
1088 *Academy of Sciences* 111, 15296–15303.

1089 Lambert C., Vidal M., Penaud A., Combourieu-Nebout N., Lebreton V., Ragueneau O.,
1090 Gregoire G., 2017. Modern palynological record in the Bay of Brest (NW France):
1091 Signal calibration for palaeo-reconstructions. *Rev. Palaeobot. Palynol.* 244, 13–25.

1092 Lewis, J., Dodge, J. D., Powell, A. J., 1990. Quaternary dinoflagellate cysts from the
1093 upwelling system off shore Peru, Hole 686B, ODP leg 112. *Proceedings of ODP*
1094 *Scientific Results*, 112, 323–327.

1095 Lézine, A.M., Duplessy, J.C., Cazet, J.P., 2005. West African monsoon variability during the
1096 last deglaciation and the Holocene: evidence from fresh water algae, pollen and
1097 isotope data from core KW31, Gulf of Guinea. *Palaeogeogr. Palaeoclimatol.*
1098 *Palaeoecol* 219, 225-237.

1099 Marcott, S. A., Clark, P. U., Padman, L., Klinkhammer, G. P., Springer, S. R., Liu, Z., et al.,
1100 2011. Ice-shelf collapse from subsurface warming as a trigger for Heinrich events.
1101 *Proceedings of the National Academy of Sciences* 108, 13415–13419.

1102 Margalef, R., 1958. Temporal succession and spatial heterogeneity in phytoplankton.
1103 *Perspectives in marine biology* 323–349.

1104 Marret, F., 1994. Distribution of dinoflagellate cysts in recent marine sediments from the east
1105 Equatorial Atlantic (Gulf of Guinea). *Rev. Palaeobot. Palynol.* 84, 1–22.

- 1106 Marret, F., Zonneveld, K.A.F., 2003. Atlas of modern organic-walled dinoflagellate cyst
1107 distribution. *Rev. Palaeobot. Palynol.* 125, 1–200.
- 1108 Marret, F., Scourse, J., Austin, W., 2004. Holocene shelf-sea seasonal stratification dynamics:
1109 A dinoflagellate cyst record from the Celtic Sea, NW European shelf. *The Holocene*
1110 14, 689-696.
- 1111 Marret, F., Bradley, L., de Vernal, A., Hardy, W., Kim, S. Y., Mudie, P., et al., 2020. From
1112 bi-polar to regional distribution of modern dinoflagellate cysts, an overview of their
1113 biogeography. *Marine Micropaleontology* 159, 101753.
- 1114 Martrat, B., Grimalt, J. O., Shackleton, N. J., de Abreu, L., Hutterli, M. A., Stocker, T. F.,
1115 2007. Four climate cycles of recurring deep and surface water destabilizations on the
1116 Iberian margin. *Science* 317, 502–507.
- 1117 Martrat, B., Jimenez-Amat, P., Zahn, R., Grimalt, J. O., 2014. Similarities and dissimilarities
1118 between the last two deglaciations and interglaciations in the North Atlantic region.
1119 *Quat. Sci. Rev.* 99, 122–134.
- 1120 Matthiessen, J., 1995. Distribution patterns of dinoflagellate cysts and other organic-walled
1121 microfossils in recent Norwegian-Greenland Sea sediments. *Mar. Micropaleontol.* 24,
1122 307–334.
- 1123 McManus, J.F., Francois, R., Gherardi, J.M., Keigwin, L.D., Drown-Leger, S., 2004. Collapse
1124 and rapid resumption of Atlantic meridional circulation linked to deglacial climate
1125 changes. *Nature* 428, 834–837.
- 1126 Ménot, G., Bard, E., Rostek, R., Weijers, W.H., Hopmans, E.C., Schouten, S., Sinninghe
1127 Damsté, J.S., 2006. Early reactivation of European rivers during the last deglaciation.
1128 *Science* 313, 1623–1625.
- 1129 Missiaen, L., Waelbroeck, C., Pichat, S., Jaccard, S. L., Eynaud, F., Greenop, R., Burke, A.
1130 2019. Improving North Atlantic marine core chronologies using ^{230}Th normalization.
1131 *Paleoceanography and paleoclimatology* 34, 1057–1073.
- 1132 Mix, A.C., Bard, E., Schneider, R., 2001. Environmental processes of the ice age: land,
1133 oceans, glaciers (EPILOG). *Quat. Sci. Rev.* 20 (4), 627—657.
- 1134 Mojtahid, M., Eynaud, F., Zaragosi, S., Scourse, J., Bourillet, J.F., Garlan, T., 2005.
1135 Palaeoclimatology and palaeohydrography of the glacial stages on Celtic and
1136 Armorican margins over the last 360 000 yrs. *Marine Geology* 224, 57–82.
- 1137 Mojtahid, M., Toucanne, S., Fentimen, R., Barras, C., Le Houedec, S., Soulet, G., et al., 2017.
1138 Changes in northeast Atlantic hydrology during Termination 1: Insights from Celtic
1139 margin's benthic foraminifera. *Quaternary Science Reviews* 175, 45–59.

1140 Morellón, M., Valero-Garcés, B., Vegas-Vilarrúbia, T., González-Sampéris, P., Romero, Ó.,
1141 et al., 2009. Late glacial and Holocene palaeohydrology in the western Mediterranean
1142 region: The Lake Estanya record (NE Spain). *Quat. Sci. Rev.* 28, 2582–2599.

1143 Moreno, A., Stoll, H.M., Jimenez-Sanchez, M., Cacho, I., Valero-Garces, B., Ito, E.,
1144 Edwards, L.R., 2010. A speleothem record of rapid climatic shifts during last glacial
1145 period from Northern Iberian Peninsula. *Glob. Planet. Chang.* 71, 218–231

1146 Morzadec-Kerfourn, M.-T., 1977. Les kystes de Dinoflagellés dans les sédiments récents le
1147 long des côtes bretonnes. *Rev. Micropaleontol.* 20, 157–166.

1148 National Oceanographic Data Centre (NODC), 2001. World Ocean Atlas.
1149 http://www.nodc.noaa.gov/OC5/WOD01/pr_wod01.html.

1150 Naughton, F., Sanchez Goñi, M.F., Desprat, S., Turon, J.-L., Duprat, J., Malaizé, B., Joli, C.,
1151 Cortijo, E., Drago, T., Freitas, M.C., 2007. Present-day and past (last 25 000 years)
1152 marine pollen signal off western Iberia. *Mar. Micropaleontol.* 62, 91–114.

1153 Naughton, F., Sanchez Goñi, M.F., Kageyama, M., Bard, E., Cortijo, E., Desprat, S., Duprat,
1154 J., Malaizé, B., Joli, C., Rostek, F., Turon, J.-L., 2009. Wet to dry climatic trend in
1155 north western Iberia within Heinrich events. *Earth Planet. Sci. Lett.* 284, 329–342.

1156 Naughton, F., Goñi, M. S., Rodrigues, T., Salgueiro, E., Costas, S., Desprat, S., et al., 2016.
1157 Climate variability across the last deglaciation in NW Iberia and its margin.
1158 *Quaternary International* 414, 9–22.

1159 Ng, H. C., Robinson, L. F., McManus, J. F., Mohamed, K. J., Jacobel, A. W., Ivanovic, R. F.,
1160 Gregoire, L.J., Chen, T., 2018. Coherent deglacial changes in western Atlantic Ocean
1161 circulation. *Nature communications* 9, 1–10.

1162 North Greenland Ice Core Project, m., 2004. High-resolution record of Northern Hemisphere
1163 climate extending into the last interglacial period. *Nature* 431, 147–151.

1164 Nygård, A., Sejrup, H.P., Haflidason, H., Leksens, W.A.H., Clark, C.D., Bigg, G.R., 2007.
1165 Extreme sediment and ice discharge from marine-based ice streams: new evidence
1166 from the North Sea. *Geology* 35, 395–398.

1167 Peck, V.L., Hall, I.R., Zahn, R., Elderfield, H., Grousset, F., Hemming, S.R., Scourse, J.D.,
1168 2006. High resolution evidence for linkages between NW European ice sheet
1169 instability and Atlantic Meridional Overturning Circulation. *Earth Planet. Sci. Lett.*
1170 243, 476–488.

1171 Penaud, A., Eynaud, F., Turon, J.L., Zaragosi, S., Marret, F., Bourillet, J.F., 2008. Interglacial
1172 variability (MIS 5 and MIS 7) and dinoflagellate cyst assemblages in the Bay of
1173 Biscay (North Atlantic). *Mar. Micropaleontol.* 68, 136–155.

- 1174 Penaud, A., Eynaud, F., Turon, J. L., Zaragosi, S., Malaizé, B., Toucanne, S., Bourillet, J. F.
1175 2009. What forced the collapse of European ice sheets during the last two glacial
1176 periods (150 ka BP and 18 ka cal BP)? Palynological evidence. *Palaeogeogr.*
1177 *Palaeoclimatol. Palaeoecol.* 281, 66–78.
- 1178 Penaud, A., Eynaud, F., Voelker, L., Helga, A., Turon, J. L., 2016. Palaeohydrological
1179 changes over the last 50 ky in the central Gulf of Cadiz: complex forcing mechanisms
1180 mixing multi-scale processes. *Biogeosciences* 13, 5357–5377.
- 1181 Penaud, A., Ganne, A., Eynaud, F., Lambert, C., Coste, P. O., Herlédan, M., et al., 2020.
1182 Oceanic *versus* continental influences over the last 7 kyrs from a mid-shelf record in
1183 the northern Bay of Biscay (NE Atlantic). *Quat. Sci. Rev.* 229, 106135.
- 1184 R Development Core Team., 2008. R: A language and environment for statistical computing.
1185 R Foundation for Statistical Computing, Vienna, Austria. ISBN 3-900051-07-0.
- 1186 Radi, T., Bonnet, S., Cormier, M. A., de Vernal, A., Durantou, L., Faubert, É., et al., 2013.
1187 Operational taxonomy and (paleo-) autecology of round, brown, spiny dinoflagellate
1188 cysts from the Quaternary of high northern latitudes. *Mar. Micropaleontol.* 98, 41–57.
- 1189 Rasmussen, S. O., Bigler, M., Blockley, S. P., Blunier, T., Buchardt, S. L., Clausen, H. B.,
1190 Cvijanovic, I., Dahl-Jensen, D., Johnsen, S. J., et al., 2014. A stratigraphic framework
1191 for abrupt climatic changes during the Last Glacial period based on three synchronized
1192 Greenland ice-core records: Refining and extending the INTIMATE event
1193 stratigraphy, *Quat. Sci. Rev.* 106, 14–28.
- 1194 Reimnitz, E., Kempama, E.W., 1987. Field observations of slush-ice generated during freeze-
1195 up in Arctic coastal waters. *Mar. Geol.* 77, 219–231.
- 1196 Rochon, A., Vernal, A.d., Turon, J.-L., Matthießen, J., Head, M., 1999. Distribution of recent
1197 dinoflagellate cysts in surface sediments from the North Atlantic Ocean and adjacent
1198 seas in relation to sea-surface parameters. *American Association of Stratigraphic*
1199 *Palynologists Contribution Series* 35, 1–146.
- 1200 Rosell-Melé, A., Comes, P., 1999. Evidence for a Warm Last Glacial Maximum in the Nordic
1201 Seas or an example of shortcomings in UK 37' and UK 37 to estimate low sea surface
1202 temperature? *Paleoceanography* 14, 770–776.
- 1203 Salgueiro, E., Naughton, F., Voelker, A.H.L., de Abreu, L., Alberto, A., Rossignol, L.,
1204 Duprat, J., Magalhães, V.H., Vaqueiro, S., Turon, J.-L., Abrantes, F., 2014. Past
1205 circulation along the western Iberian margin: a time slice vision from the Last Glacial
1206 to the Holocene. *Quat. Sci. Rev.* 106, 316–329.

1207 Stanford, J.D., Rohling, E.J., Hunter, S.E., Roberts, A.P., Rasmussen, S.O., Bard, E.,
1208 McManus, J., Fairbanks, R.G., 2006. Timing of mwp-1a and climate responses to
1209 meltwater injections. *Paleoceanography* 21, PA4103.

1210 Stanford, J. D., Rohling, E. J., Bacon, S., Roberts, A. P., Grousset, F. E., Bolshaw, M., 2011.
1211 A new concept for the paleoceanographic evolution of Heinrich event 1 in the North
1212 Atlantic. *Quat. Sci. Rev.* 30, 1047–1066.

1213 Sutton, R., Allen, M., 1997. Decadal predictability of North Atlantic sea surface temperature
1214 and climate. *Nature* 388, 563-567.

1215 Svensson, A., Andersen, K.K., Bigler, M., Clausen, H.B., Dahl-Jensen, D., Davies, S.M.,
1216 Johnsen, S.J., Muscheler, R., Rasmussen, S.O., Röthlisberger, R., Steffensen, J.P.,
1217 Vinther, B.M., 2006. The Greenland ice core chronology 2005, 15-42 ka. Part 2:
1218 comparison to other records. *Quat. Sci. Rev.* 25, 23-24.

1219 Svensson, A., Andersen, K. K., Bigler, M., Clausen, H. B., Dahl- Jensen, D., Davies, S. M., J
1220 ohnson, S. J., Muscheler, R., Parrenin, F., Rasmussen, S. O., Röthlisberger, R.,
1221 Seierstad, I., Steffensen, J. P., Vinther, B. M., 2008. A 60 000-year Greenland
1222 stratigraphic ice core chronology. *Clim. Past.* 4, 47–57.

1223 Toucanne, S., Zaragosi, S., Bourillet, J.F., Naughton, F., Cremer, M., Eynaud, F., Dennielou,
1224 B., 2008. Activity of the turbidite levees of the Celtic-armoric margin (Bay of
1225 Biscay) during the last 30,000 years: imprints of the last European deglaciation and
1226 Heinrich events. *Mar. Geol.* 247, 84–103.

1227 Toucanne, S., Zaragosi, S., Bourillet, J.F., Cremer, M., Eynaud, F., Turon, J.L., Fontanier, C.
1228 Van Vliet Lanoë, B., Gibbard, P., 2009. Timing of massive ‘Fleuve Manche’
1229 discharges over the last 350 kyr: insights into the European Ice Sheet oscillations and
1230 the European drainage network from MIS 10 to 2. *Quat. Sci. Rev.* 28, 1238–1256.

1231 Toucanne, S., Zaragosi, S., Bourillet, J. F., Marieu, V., Cremer, M., Kageyama, M., et al.,
1232 2010. The first estimation of Fleuve Manche palaeoriver discharge during the last
1233 deglaciation: Evidence for Fennoscandian ice sheet meltwater flow in the English
1234 Channel ca 20–18 ka ago. *Earth Planet. Sci. Lett.* 290, 459–473.

1235 Toucanne, S., Zaragosi, S., Bourillet, J. F., Dennielou, B., Jorry, S. J., Jouet, G., Cremer, M.
1236 2012. External controls on turbidite sedimentation on the glacially-influenced
1237 Armorican margin (Bay of Biscay, western European margin). *Mar. Geol.* 303, 137–
1238 153.

- 1239 Toucanne, S., Soulet, G., Freslon, N., Jacinto, R. S., Dennielou, B., Zaragosi, S., et al., 2015.
1240 Millennial-scale fluctuations of the European Ice Sheet at the end of the last glacial,
1241 and their potential impact on global climate. *Quat. Sci. Rev.* 123, 113–133.
- 1242 Toucanne, S., Soulet, G., Vázquez Riveiros, N., Boswell, S. M., Dennielou, B., Waelbroeck,
1243 C., ... et al., 2021. The North Atlantic Glacial Eastern Boundary Current as a Key
1244 Driver for Ice-Sheet—AMOC Interactions and Climate Instability. *Paleoceanography*
1245 and *Paleoclimatology* 36, e2020PA004068.
- 1246 Turon, J. L., 1984. Le palynoplancton dans l'environnement actuel de l'Atlantique Nord-
1247 oriental. Evolution climatique et hydrologique depuis le dernier maximum glaciaire.
1248 Mémoires de l'Institut de Géologie du Bassin d'Aquitaine, 17, 313 pp.
- 1249 Turon, J.-L., Londeix, L., 1988. Dinoflagellate assemblages in the western Mediterranean,
1250 Alboran sea: evidence of the evolution of palaeoenvironments since the last glacial
1251 maximum [Les assemblages de kystes de Dinoflagelles en Méditerranée occidentale
1252 (Mer d'Alboran): mise en évidence de l'évolution des palaeoenvironnements depuis le
1253 dernier maximum glaciaire.]. *Bulletin – Centres de Recherche Exploration- Production*
1254 *Elf-Aquitaine* 12, 313–344.
- 1255 Turon, J.L., Lézine, A.M., Denèfle, M., 2003. Land-sea correlations for the last glaciation
1256 inferred from a pollen and dinocyst record from the Portuguese margin. *Quat. Res.* 59,
1257 88–96.
- 1258 Van Nieuwenhove, N., Pospelova, V., de Vernal, A., Rochon, A., 2020. A historical
1259 perspective on the development of the Northern Hemisphere modern dinoflagellate
1260 cyst database. 101824.
- 1261 Versteegh, G. J., Zonneveld, K. A., 1994. Determination of (palaeo-) ecological preferences of
1262 dinoflagellates by applying detrended and canonical correspondence analysis to Late
1263 Pliocene dinoflagellate cyst assemblages of the south Italian Singa section. *Rev.*
1264 *Palaeobot. Palynol.* 84, 181–199.
- 1265 Voelker, A. H., 2002. Global distribution of centennial-scale records for Marine Isotope Stage
1266 (MIS) 3: a database. *Quat. Sci. Rev.* 21, 1185–1212.
- 1267 Waelbroeck, C., Lougheed, B. C., Riveiros, N. V., Missiaen, L., Pedro, J., Dokken, T., et al.,
1268 2019. Consistently dated Atlantic sediment cores over the last 40 thousand years.
1269 *Scientific data* 6, 1–12.
- 1270 Wall, D., Dale, B., Lohmann, G.P., Smith, W.K., 1977. The environment and climatic
1271 distribution of dinoflagellate cysts in modern marine sediments from regions in the
1272 north and south Atlantic oceans and adjacent seas. *Mar. Micropaleontol.* 2, 121–200.

1273 Wary, M., Eynaud, F., Sabine, M., Zaragosi, S., Rossignol, L., Malaize, B., et al., 2015.
1274 Stratification of surface waters during the last glacial millennial climatic events: a key
1275 factor in subsurface and deep-water mass dynamics. *Clim. Past.* 11, 1507.

1276 Weaver, A.J., Saenko, O.A., Clark, P.U., Mitrovica, J.X., 2003. Meltwater pulse 1A from
1277 Antarctica as a trigger of the Bølling-Allerød warm interval. *Science* 299, 1709-1713.

1278 Weinelt, M., Sarnthein, M., Pflaumann, U., Schulz, H., Jung, S., Erlenkeuser, H., 1996. Ice-
1279 free Nordic Seas during the Last Glacial Maximum? Potential sites of deepwater
1280 formation. *Paleoclimates* 1, 283–309.

1281 Woerther, P., 2013. VT 133 /MERIADZEK cruise, RV Marion Dufresne.

1282 Zaragosi, S., Auffret, G. A., Faugères, J. C., Garlan, T., Pujol, C., Cortijo, E., 2000.
1283 Physiography and recent sediment distribution of the Celtic Deep-Sea Fan, Bay of
1284 Biscay. *Mar. Geol.* 169, 207–237.

1285 Zaragosi, S., Eynaud, F., Pujol, C., Auffret, G., Turon, J.-L., Garlan, T., 2001. Initiation of the
1286 European deglaciation as recorded in the northwestern Bay of Biscay slope
1287 environments (Meriadzek Terrace and Trevelyan Escarpment): a multi-proxy
1288 approach. *Earth Planet. Sci. Lett.* 188, 493–507.

1289 Zaragosi, S., Bourillet, J.F., Eynaud, F., Toucanne, S., Denhard, B., Van Toer, A., Lanfumeu,
1290 V., 2006. The impact of the last European deglaciation on the deepsea turbidite
1291 systems of the Celtic-Armorican margin (Bay of Biscay). *Geo-Marine Letters* 26,
1292 317–329.

1293 Zonneveld, K.A.F., 1997. New species of organic walled dinoflagellate cysts from modern
1294 sediments of the Arabian Sea (Indian Ocean). *Rev. Palaeobot. Palynol.* 97, 319–337

1295 Zonneveld, K.A.F., Hoek, R.P., Brinkhuis, H., Willems, H., 2001. Geographical distributions
1296 of organic-walled dinoflagellate cysts in surficial sediments of the Benguela upwelling
1297 region and their relationship to upper ocean conditions. *Progress in Oceanography* 48,
1298 25–72.

1299 Zonneveld, K. A., Versteegh, G., Kodrans-Nsiah, M., 2008. Preservation and organic
1300 chemistry of Late Cenozoic organic-walled dinoflagellate cysts: A review. *Marine*
1301 *Micropaleontology* 68, 179–197.

1302 Zonneveld, K.A.F., Marret, F., Versteegh, G.J.M., Bogus, K., Bonnet, S., Bouimetarhan, I., et
1303 al., 2013. Atlas of modern dinoflagellate cyst distribution based on 2405 data points
1304 *Rev. Palaeobot. Palynol.* 191, 1–197.

1305 Zumaque, J., Eynaud, F., de Vernal, A., 2017. Holocene paleoceanography of the Bay of
1306 Biscay: evidence for west-east linkages in the North Atlantic based on dinocyst data.
1307 *Palaeogeogr. Palaeoclimatol. Palaeoecol.* 468, 403–413.

Table 1

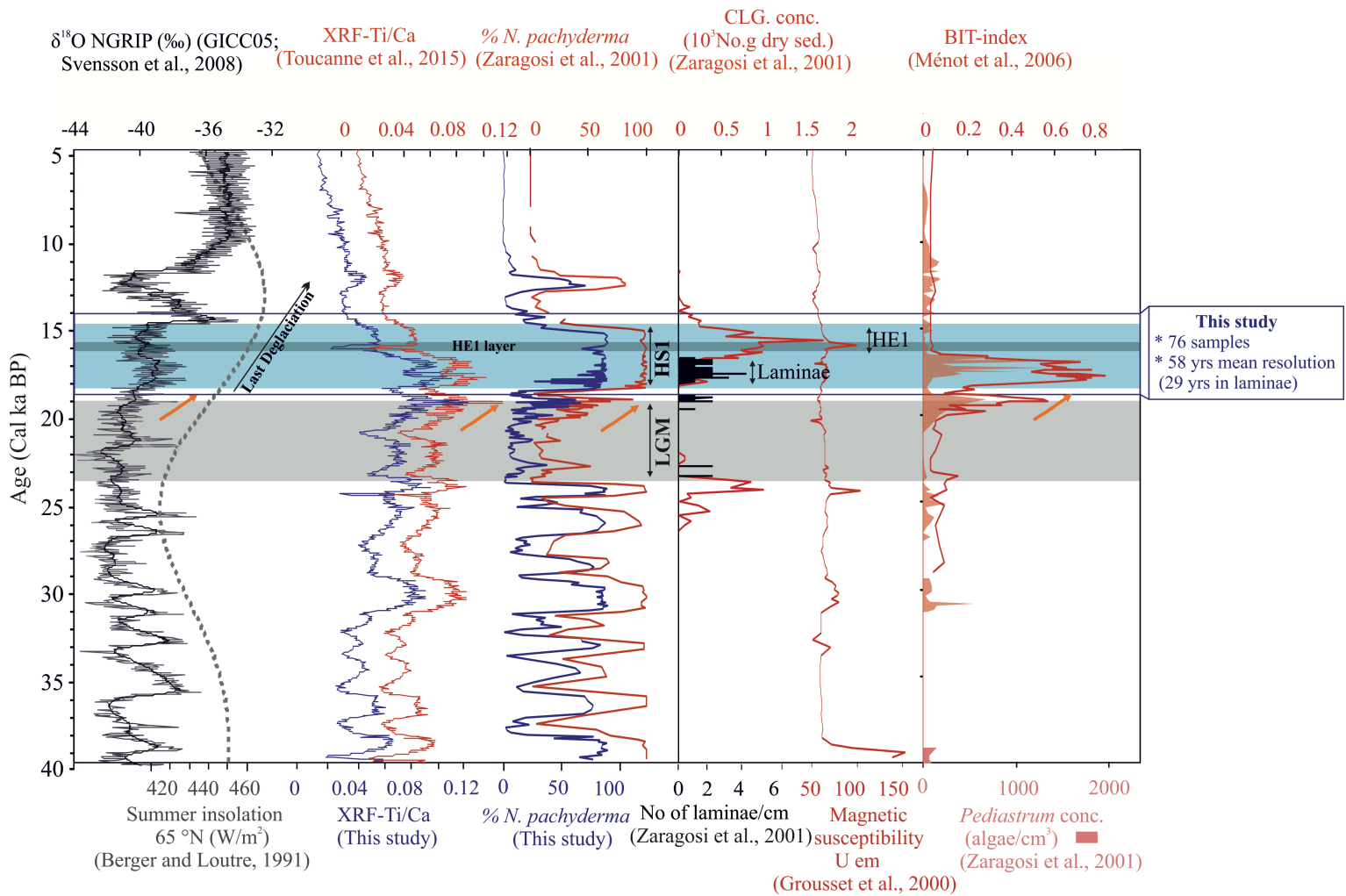
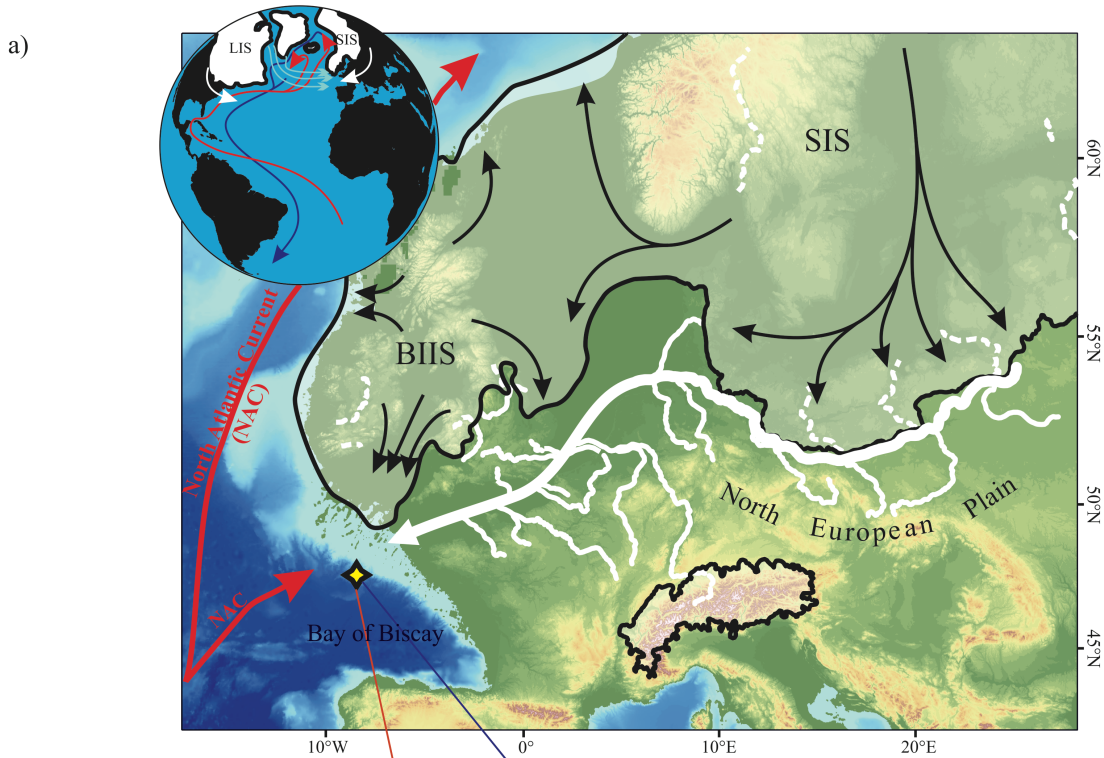
Core name	Geographic coordinates Depth (m)	Dinocyst assemblages	Ti/Ca-XRF ratio	% <i>N.pachydermas</i>	IRD conc (No g dry sed)	No Laminae/cm	BIT index + % COT
MD13-3438 Studied core	47° 27' N 8° 27' W 2180 m	This study	S. Toucanne in this study	L. Rossignol in this study	No data	No data	No data
MD95-2002 Reference core	47°27' N 8°32' W 2174 m	Eyraud, 1999 ; Zaragosi et al., 2001 ; Eyraud et al., 2012	Toucanne et al., 2015	Zaragosi et al., 2001 ; Eyraud et al., 2009	Zaragosi et al., 2001	Zaragosi et al., 2001	Ménot et al., 2006

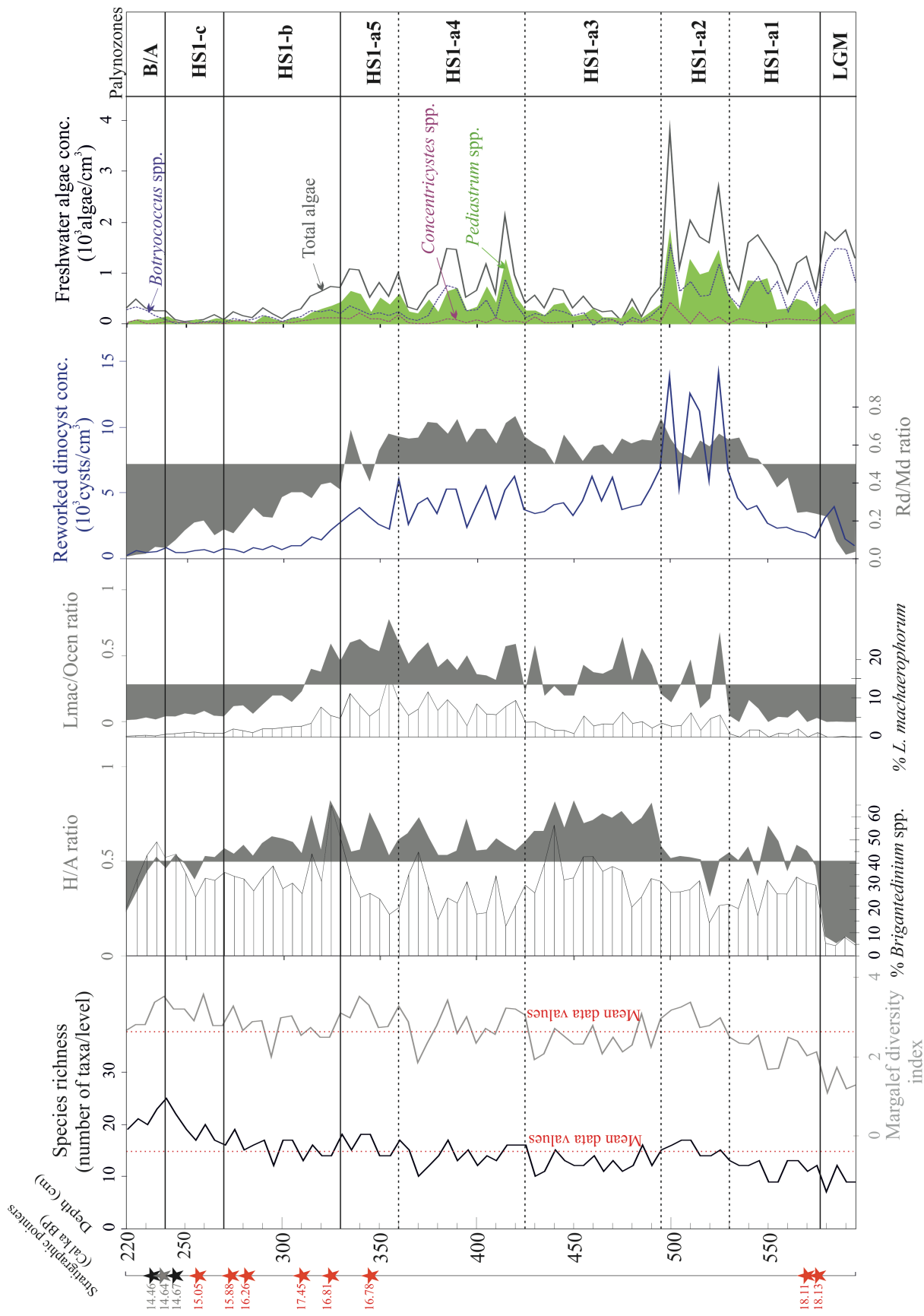
Table 2

Tie points MD95-2002	Depth MD95-2002 (cm)	Equivalent depth MD13-3438 (cm)	Age cal BP (Toucanne et al.,2015)
Top core	0	0	1629
End YD	190	126	11488
Onset YD	262	170	12442
End HS1	390	242	14699
HS1-5	455	277	15908
HS1-4	515	314	16482
HS1-3(2)	548	324	16724
HS1-3	690	428	17388
HS1-2	745	475	17559
Onset HS1	865	567	18100
End LGM	940	619	18570
LGM-6	970	640	18739
LGM-5	1000	663	18904
LGM-4	1040	697	19127
LGM-3	1145	788	19807
LGM-2	1260	881	21077
LGM-1	1340	952	22788
Onset LGM	1355	960	23001
End HS2	1375	981	23185
HS2-4	1415	1011	23560
HS2-3	1460	1050	24249
HS2-2	1495	1084	25031
Onset HS2	1550	1123	26551
End GI-3	1573	1155	27186
Onset GI-3	1593	1179	27720
End HS3 / Onset GI-4	1640	1218	28953
mid HS3	1695	1287	30116
Onset HS3	1745	1339	31050
Onset GI-5	1793	1389	32419
Onset-GI-7	1858	1458	35694
End GI-8	1880	1482	36900
End HS4 / Onset GI-8	1906	1511	37908
mid-HS4	1968	1575	39300

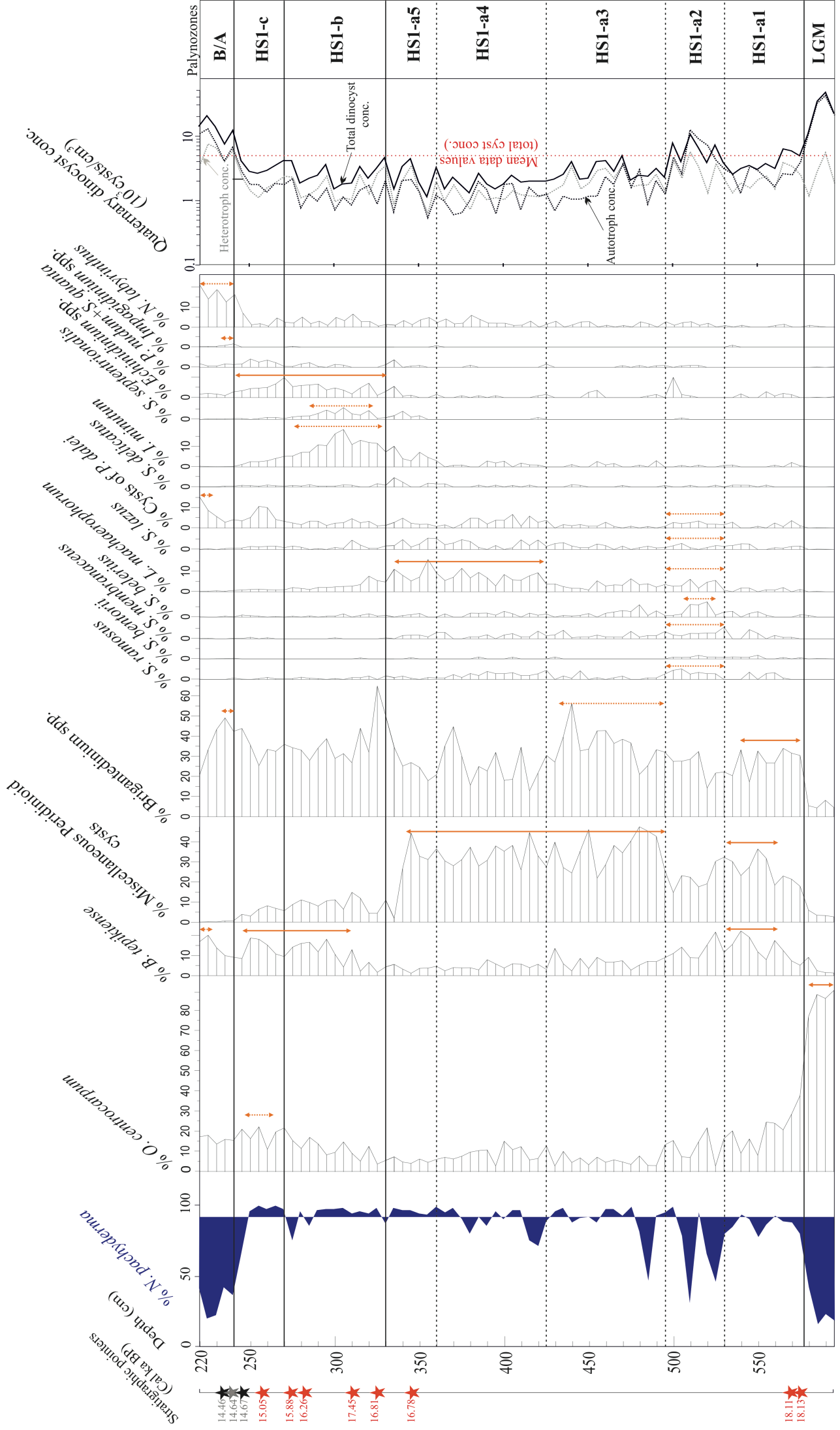
Table 3

	Name of taxa	Abbreviation
Autotrophic taxa	<i>Bitectatodinium tepikiense</i>	Btep
	<i>Impagidinium aculeatum</i>	Iacu
	<i>Impagidinium pallidum</i>	Ipal
	<i>Impagidinium paradoxum</i>	Ipar
	<i>Impagidinium patulum</i>	Ipat
	<i>Impagidinium sphaericum</i>	Isph
	<i>Lingulodinium machaerophorum</i>	Lmac
	<i>Nematosphaeropsis labyrinthus</i>	Nlab
	<i>Operculodinium centrocarpum</i>	Ocen
	<i>Operculodinium janduchenei</i>	Ojan
	<i>Polysphaeridium zoharyi</i>	Pzoh
	<i>Spiniferites membranaceus</i>	Smem
	<i>Spiniferites delicatus</i>	Sdel
	<i>Spiniferites elongatus</i>	Selo
	<i>Spiniferites ramosus</i>	Sram
	<i>Spiniferites belerius</i>	Sbel
	<i>Spiniferites bentorii</i>	Sben
	<i>Spiniferites lazus</i>	Slaz
	<i>Spiniferites mirabilis</i>	Smir
	<i>Spiniferites</i> spp.	Sspp
<i>Spiniferites septentrionalis</i>	Ssep	
Cyst of <i>Pentapharsodinium dalei</i>	Pdal	
Heterotrophic taxa	<i>Islandinium minutum</i>	Imin
	<i>Brigantedinium</i> spp.	Bspp
	<i>Quinquecuspis</i> spp.	Qspp
	<i>Lejeunecysta</i> spp.	Lspp
	<i>Dubridinium</i> spp.	Dspp
	<i>Votadinium</i> spp.	Vspp
	<i>Selenopemphix quanta</i>	Squa
	Cyst of <i>Protoperidinium nudum</i>	Pnud
	<i>Echinidinium</i> spp.	Espp

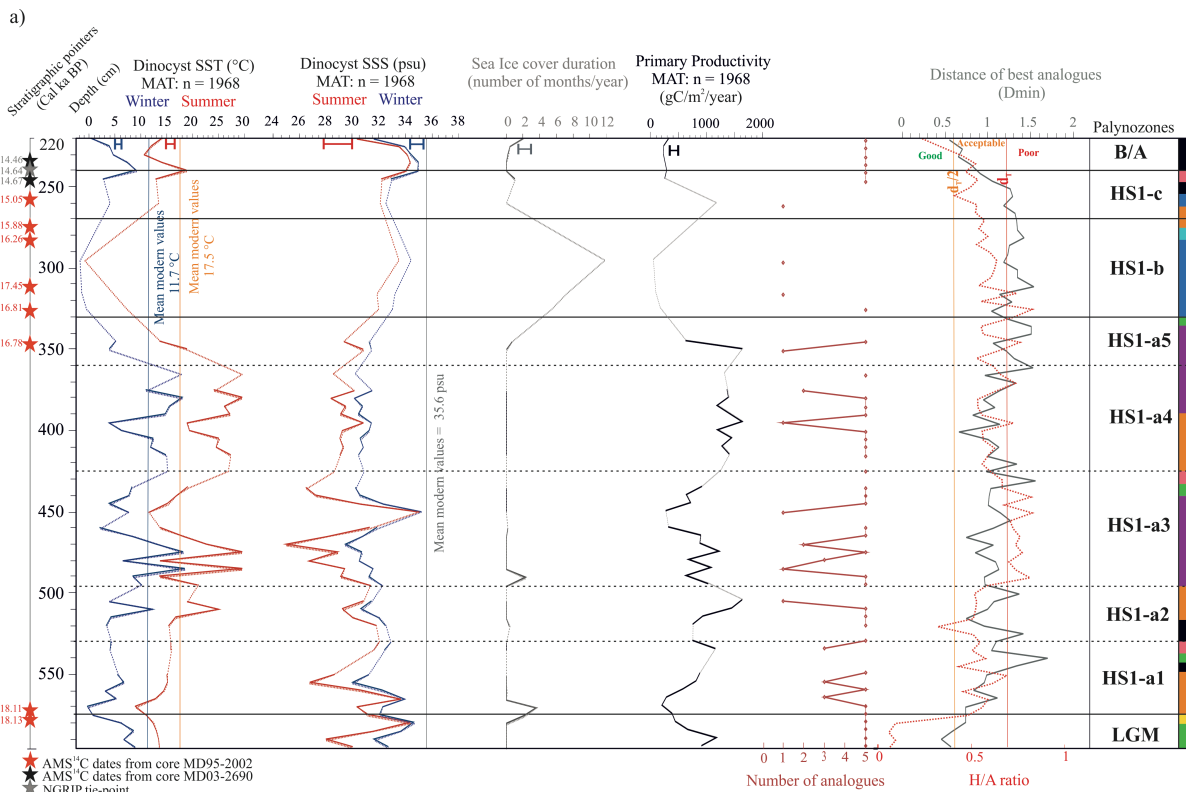




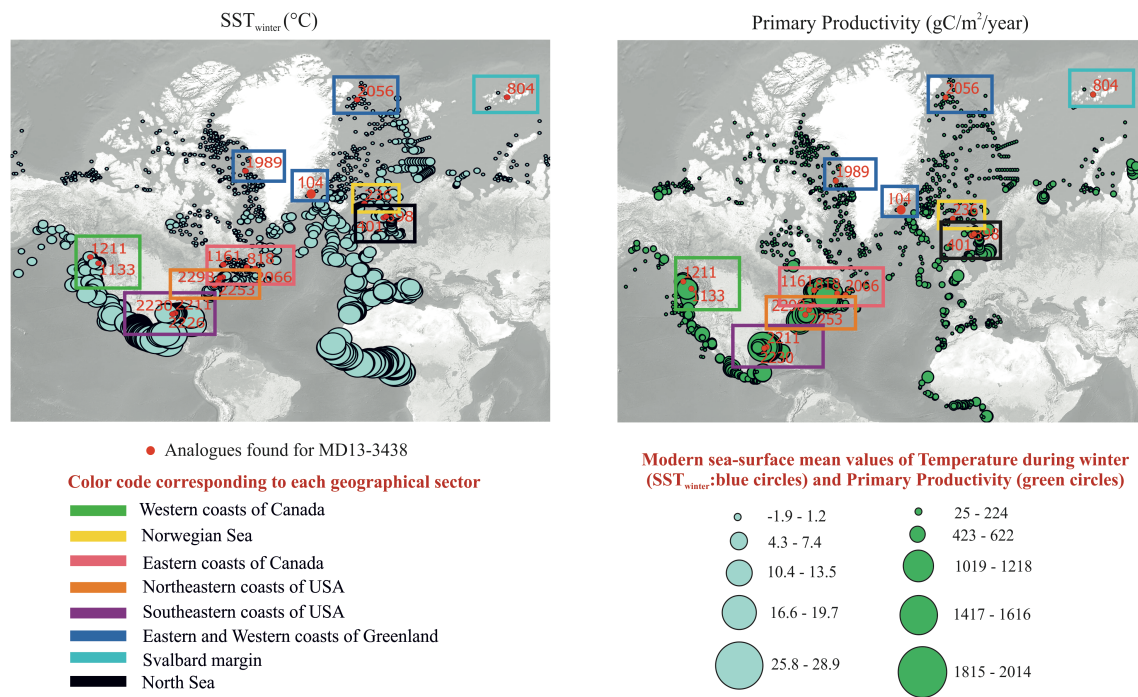
* AMS¹⁴C dates from core MD95-2002
 * AMS¹⁴C dates from core MD03-2690
 * NGRIP tie-point

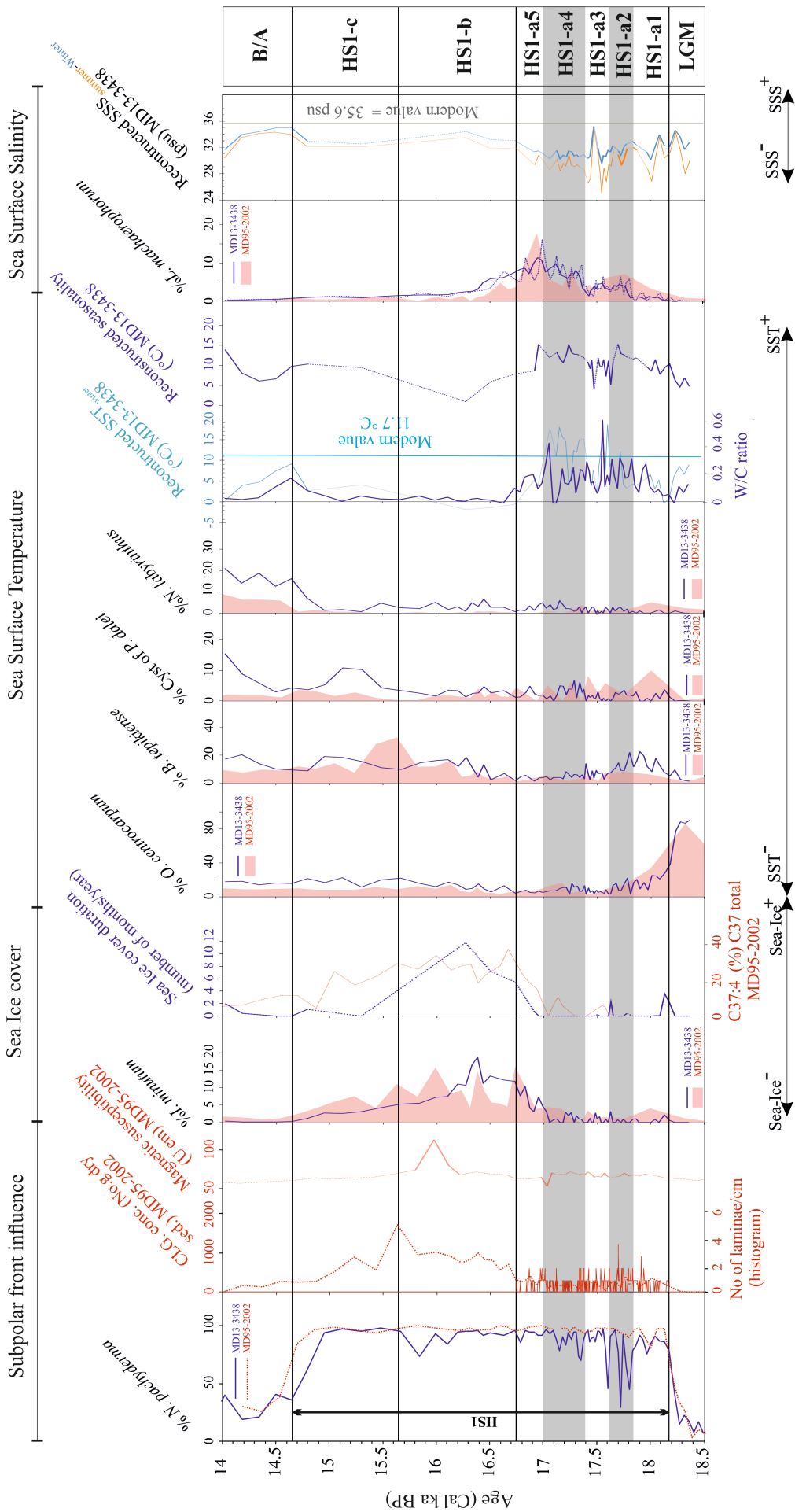


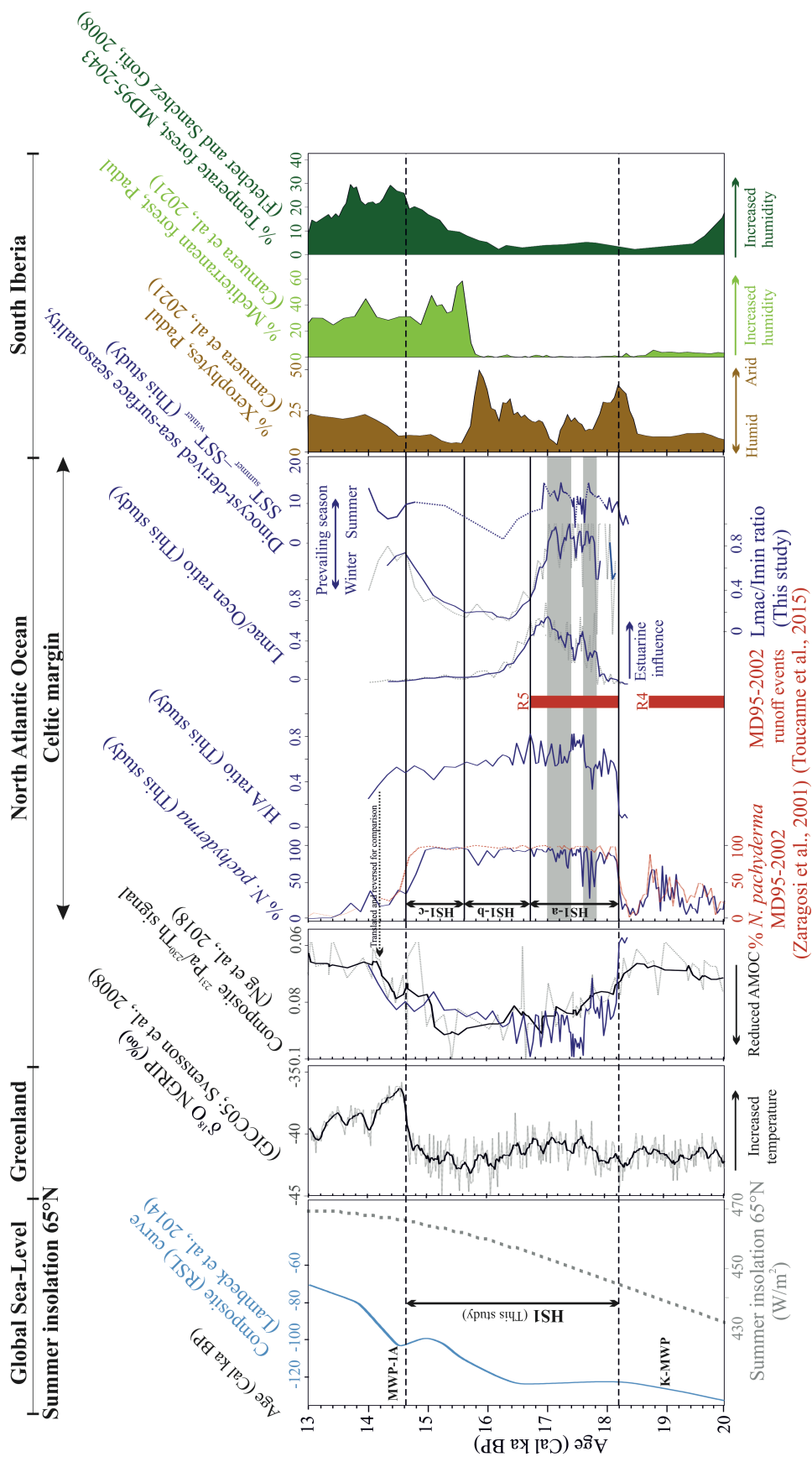
★ AMS ¹⁴C dates from core MID95-2002
 ★ AMS ¹⁴C dates from core MID03-2690
 ★ NGRIP tie-point



b) Database n=1968 (de Vernal et al., 2020)

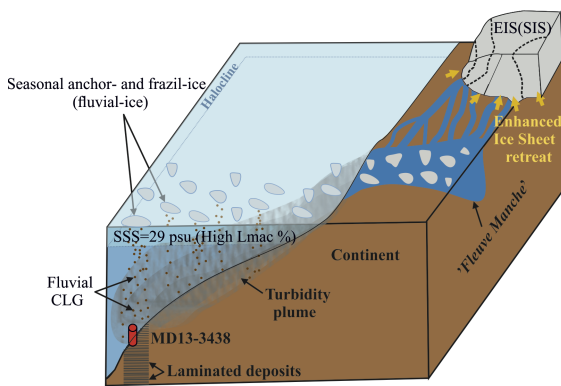




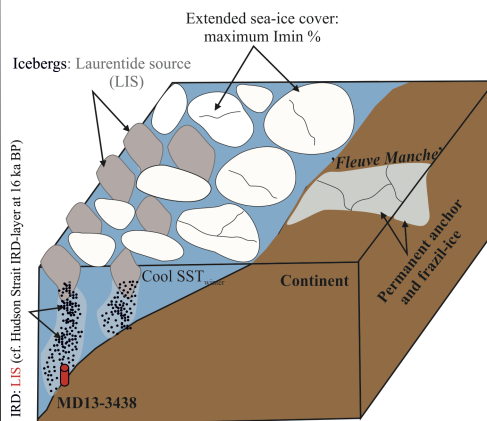


HS1-a: Laminated interval (18.2 - 16.7 ka BP)

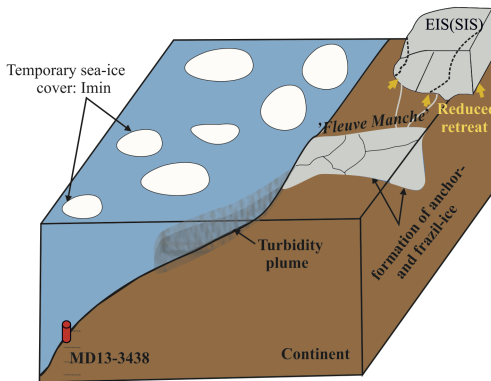
Summer-prevailing mode
(HS1-a2, HS1-a4)



HS1-b: Early-HE1 (16.7- 15.6 ka BP)



Winter-prevailing mode
(HS1-a1, HS1-a3, HS1-a5)



HS1-c: Late-HE1 (15.6- 14.6 ka BP)

